JACS
JOURNAL OF THE AMERICAN CHEMICAL SOCIETY
Article
pubs.acs.org/JACS

Self-Assembled Molecular Gear: A 4:1 Complex of Rh(III)Cl Tetraarylporphyrin and Tetra(*p*-pyridyl)cavitand

Munechika Nakamura,[†] Kazuki Kishimoto,[†] Yasuhiro Kobori,*[,‡] Tomoka Abe,[‡] Kenji Yoza,[§] and Kenji Kobayashi*[,†]

[†]Department of Chemistry, Faculty of Science, Shizuoka University, 836 Ohya, Suruga-ku, Shizuoka 422-8529, Japan
[‡]Department of Chemistry, Graduate School of Science, Kobe University, 1-1 Rokkodaicho, Nada-ku, Kobe 657-8501, Japan
[§]Bruker axs, 3-9-B Moriya, Kanagawa-ku, Yokohama 221-0022, Japan

Supporting Information

ABSTRACT: The components of a 4:1 mixture of Rh(III)Cl tetrakis(4-methylphenyl)porphyrin **1** and a bowl-shaped tetra(4-pyridyl)cavitand **4** self-assemble into a 4:1 complex $\mathbf{1}_4$•**4** via Rh−pyridyl axial coordination bonds. The single-crystal X-ray diffraction analysis and variable-temperature (VT) ^{1}H NMR study of $\mathbf{1}_4$•**4** indicated that $\mathbf{1}_4$•**4** behaves as a quadruple interlocking gear with an inner space, wherein (i) four subunits-**1** are gear wheels and four *p*-pyridyl groups in subunit-**4** are axes of gear wheels, (ii) one subunit-**1** and two adjacent subunits-**1** interlock with one another cooperatively, and (iii) four subunits-**1** in $\mathbf{1}_4$•**4** rotate quickly at 298 K on the NMR time scale. Together, the extremely strong porphyrin-Rh−pyridyl axial coordination bond, the rigidity of the methylene-bridge cavitand as a scaffold of the pyridyl axes, and the cruciform arrangement of the interdigitating *p*-tolyl groups as the teeth moiety of the gear wheels in the assembling $\mathbf{1}_4$-unit make $\mathbf{1}_4$•**4** function as a quadruple interlocking gear in solution. The gear function of $\mathbf{1}_4$•**4** was also supported by the rotation behaviors of other 4:1 complexes: $\mathbf{2}_4$•**4** and $\mathbf{3}_4$•**4** obtained from Rh(III)Cl tetrakis[4-(4-methylphenyl)phenyl]porphyrin **2** or Rh(III)Cl tetrakis(3,5-dialkoxyphenyl)porphyrin **3** and **4** also served as quadruple interlocking gears, whereas $\mathbf{1}_4$•**5** obtained from **1** and tetrakis[4-(4-pyridyl)phenyl]cavitand **5** did not behave as a gear. The results of activation parameters ($\Delta H^{\ddagger}$, $\Delta S^{\ddagger}$, and $\Delta G^{\ddagger}$) obtained from Eyring plots based on line-shape analysis of the VT ^{1}H NMR spectra of $\mathbf{1}_4$•**4**, $\mathbf{2}_4$•**4**, and $\mathbf{3}_4$•**4** also support the interlocking rotation (geared coupled rotation) mechanism.

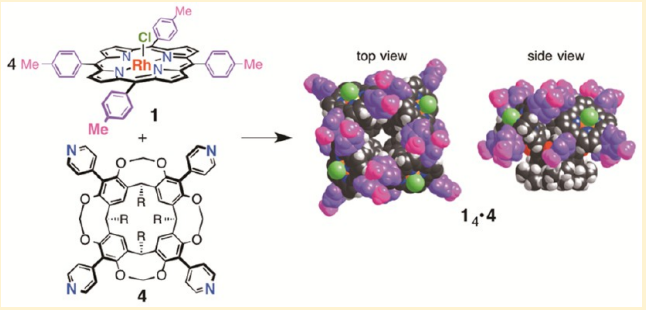

INTRODUCTION

Porphyrin derivatives have been widely used as building blocks for functional supramolecular architectures, owing to their particular electronic and photophysical properties as well as catalytic properties.[1] Metalloporphyrin−pyridine axial coordination bonds are reliable supramolecular synthons for self-assembled porphyrin architectures.[1−4] Along this line, combinations of metalloporphyrins and *meso*-tetra(*p*- or *m*-pyridyl)-porphyrin have been used for self-assembled multiporphyrin arrays directed to synthetic models of light-harvesting antennas in a photosynthetic process.[5] Molecular machines are another interesting topic in supramolecular chemistry.[6] In the 1980s, triptycene-based molecular gears, the teeth of which mesh together, were reported independently by Mislow and Iwamura.[6a] Since their pioneering work, chemists have been fascinated for decades with molecular structures that permit internal mechanical motion at various degrees of complexity, from random flipping to geared coupled motion. It is known that Rh(III)Cl *meso*-tetraarylporphyrin very tightly binds pyridyl compounds as an axial ligand.[4] This type of complex has been used as a building block for a rotaxane[7] and a molecular gear.[8] Multicomponent machinery based on supramolecular strategy represents a particular challenge.[8,9] However, molecular gear systems coupled with four gear wheels (rotors) have been almost unknown.[8,10,11]

Tetra(4-pyridyl)cavitand **4** possesses a bowl-shaped aromatic cavity with rigid conformation and four *p*-pyridyl groups oriented in a divergent and oblique direction with C_{4v} symmetry and has been used as a building block for self-assembled capsules.[12] In the molecular model of **4** (R = CH_3) calculated at the B3LYP/6-31G(d) level, the tilt angle of the *p*-pyridyl groups to the cavitand scaffold is 119°, and the N···N atomic distances between two *p*-pyridyl groups at the adjacent and diagonal positions are 8.7 and 12.3 Å, respectively. The present work is concerned with a combination of *meso*-tetrakis(4-methylphenyl)porphyrinato Rh(III)Cl **1**[13] as a gear wheel and tetra(4-pyridyl)cavitand **4** as a rigid scaffold and a multipyridyl axial ligand. Our attention has been focused on whether **1** and **4** self-assemble into 4:1 complex $\mathbf{1}_4$•**4** via Rh−

Received: July 14, 2016
Published: September 13, 2016

DOI: 10.1021/jacs.6b07284
J. Am. Chem. Soc. 2016, 138, 12564−12577

Scheme 1. Self-Assembly of a 4:1 Mixture of 1 and 4 into 1_4•4 through Rh−Pyridyl Axial Coordination Bonds

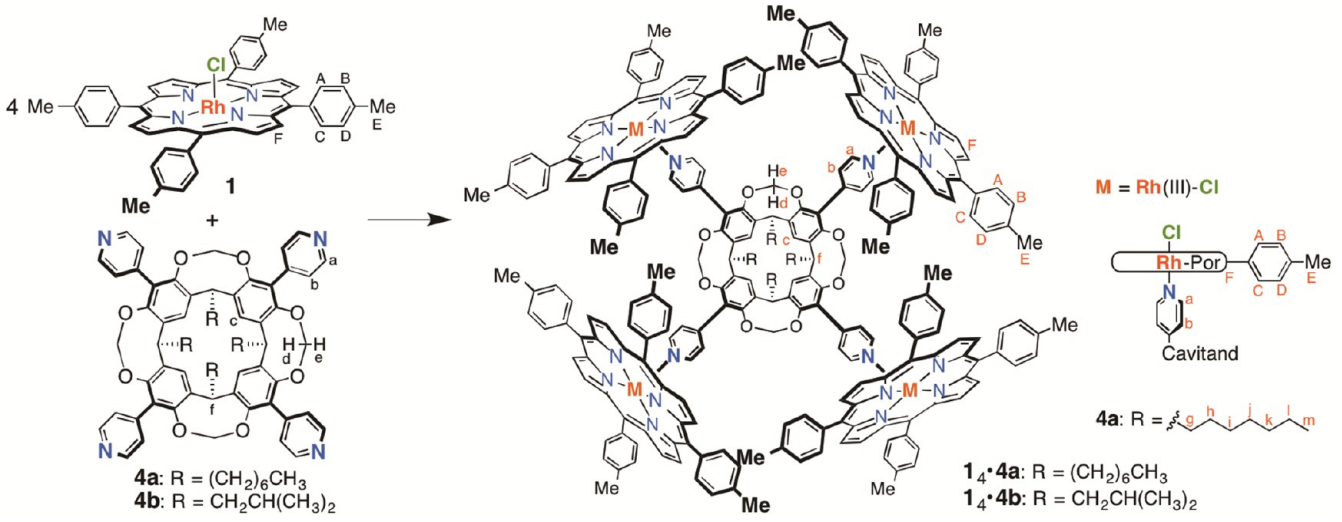

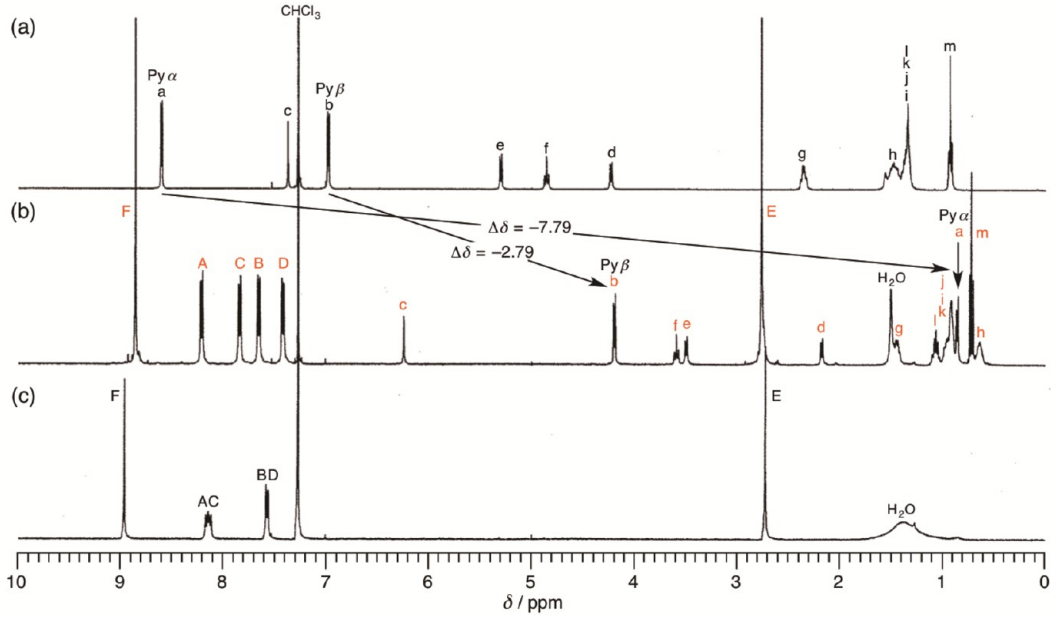

Figure 1. ^{1}H NMR spectra (400 MHz, $CDCl_3$, 298 K): (a) **4a** alone, (b) 1_4•**4a** ([**1**] = 8 mM and [**4a**] = 2 mM), and (c) **1** alone. The signals marked "A−F" and "a−m" are assigned in Scheme 1.

pyridyl axial coordination bonds despite steric congestion between the adjacent subunits-**1** because of the relatively short distance between the adjacent *p*-pyridyl groups in **4** and on whether this complex if formed behaves as a self-assembled molecular gear and/or a self-assembled capsule. This approach would be of importance because one can put four gear wheels simultaneously on a platform in a proximate fashion to construct molecular gears. Here, we report the formation of 1_4•**4** as a quadruple interlocking gear with an inner space (Scheme 1) revealed by X-ray crystallographic analysis and variable-temperature (VT) ^{1}H NMR study. The gear function of 1_4•**4** was also supported by the rotation behaviors of other 4:1 complexes 2_4•**4**, 3_4•**4**, and 1_4•**5** and by the results of activation parameters obtained from Eyring plots based on line-shape analysis of the VT ^{1}H NMR spectra of 1_4•**4**, 2_4•**4**, and 3_4•**4**. This is the first example of a quadruple interlocking gear and the use of cavitand as multiple axes of molecular gear. We also describe a chiral structure of 1_4•**4** in the single crystals.

RESULTS AND DISCUSSION

Formation of 1_4•4a in Solution. The ^{1}H NMR spectrum of a 4:1 mixture of Rh(III)Cl porphyrin **1** and pyridyl-cavitand **4a** (R = $(CH_2)_6CH_3$)[12a] in $CDCl_3$ at 298 K showed formation of a highly symmetrical single species and the complete disappearance of the signals of free **1** and free **4a** (Figure 1). This result undoubtedly indicates the quantitative formation of a 4:1 complex 1_4•**4a** via Rh−pyridyl axial coordination bonds (Scheme 1). The signal assignments of 1_4•**4a** were confirmed by the ^{1}H−^{1}H COSY and 2D NOESY spectra (Figures S6 and S7). In the ^{1}H NMR spectrum of 1_4•**4a** (Figure 1b), the signals of the Py*α*-proton (signal a) and Py*β*-proton (b), the cavitand aromatic proton (c), and the inner proton (d) and outer proton (e) of the methylene bridge rim (O−$CH_{in}H_{out}$−O) of subunit-**4a** were shifted upfield by 7.79, 2.79, 1.48, 2.06, and 1.81 ppm, respectively, relative to those of free **4a**, owing to the ring-current effect of subunit-**1**. In particular, the extremely large

DOI: 10.1021/jacs.6b07284
J. Am. Chem. Soc. 2016, 138, 12564−12577

upfield shift of the Pyα-proton signal ($\Delta\delta$ = −7.79 ppm) is concrete evidence for the Rh−pyridyl axial coordination bond between subunit-**1** and subunit-**4a**.[4,7,8] The ^{1}H NMR signals of the pyrrole-βH (signal F) and the CH_3 group (E) of the *p*-tolyl group in subunit-**1** appeared as one singlet signal ($\Delta\delta$ = −0.11 and +0.04 ppm relative to those of free **1**), namely, the four subunits-**1** in $\mathbf{1}_4$•**4a** were observed as an averaged form. This result indicates that rotations of the four subunits-**1** about the respective Rh−pyridyl axial coordination bond are fast on the NMR time scale at room temperature (vide infra). On the other hand, the two *ortho*-protons and the two *meta*-protons on each *p*-tolyl group of subunit-**1** were nonequivalent by the effect of Cl−Rh−pyridyl bonds,[5a,c,7,8] namely, the signals of the *o*- and *m*-protons of the *p*-tolyl group were observed as four doublet signals in total (see also Figure S5). This result indicates that rotation about the C−C bond between the porphyrin ring and the *p*-tolyl group is slow on the NMR time scale. The signals of *o*- and *m*-protons (signals C and D) on the Rh−pyridyl side of $\mathbf{1}_4$•**4a** were shifted upfield by 0.31 and 0.14 ppm, respectively, relative to those of free **1**, and the signals of *o*- and *m*-protons (A and B) on the Rh−Cl side of $\mathbf{1}_4$•**4a** were slightly shifted downfield by 0.06 and 0.09 ppm, respectively, relative to those of free **1**.

The formation of $\mathbf{1}_4$•**4a** was also confirmed by changing the stoichiometry upon mixing **1** with **4a** (Figures S8 and S9). The ^{1}H NMR spectrum of a 2:1 mixture of **1** and **4a** in $CDCl_3$ at 298 K showed a mixture of $\mathbf{1}_4$•**4a**, free **4a**, and other species (Figures S8c and S9a). This mixture remained unchanged after 1 day at room temperature (Figure S9b). However, after heating this mixture at 50 °C for 1 day, the spectrum changed and showed the complete disappearance of the signals of $\mathbf{1}_4$•**4a** and free **4a** and the increase of the signals of other species, which could be a mixture of **1**•**4a**, two kinds of $\mathbf{1}_2$•**4a** (two subunits-**1** are placed at the adjacent and diagonal positions), and $\mathbf{1}_3$•**4a** (Figure S9d,b). These results suggest that $\mathbf{1}_4$•**4a** obtained from a 2:1 mixture of **1** and **4a** is a kinetic product. In contrast, the ^{1}H NMR spectrum of a 5:1 mixture of **1** and **4a** in $CDCl_3$ at 298 K showed a 1:1 mixture of $\mathbf{1}_4$•**4a** and free **1** (Figure S8g), wherein the signals of $\mathbf{1}_4$•**4a** and free **1** were independently observed and remained unchanged even after heating this mixture at 50 °C for 1 day. Thus, upon mixing **1** and **4a** in a 4:1 ratio (Figure S8e), $\mathbf{1}_4$•**4a** is thermodynamically stable and quantitatively formed as a single species.

In the ^{1}H NMR spectra of a mixture of $\mathbf{1}_4$•**4a** and a small amount of free **1** in $CDCl_2CDCl_2$ at 298−358 K (Figure S10), the chemical shift of the Pyβ-proton (b) of subunit-**4a** remained completely unchanged even at 358 K,[14] although the four signals of *o*- and *m*-protons (A−D) on each *p*-tolyl group of subunit-**1** became broadened at 328 K and coalesced at 348 K. Furthermore, the chemical shifts and integrations of the signals of the pyrrole-βH (F) and the CH_3 group (E) of the *p*-tolyl group of subunit-**1** and those of free **1** also remained completely unchanged even at 358 K. These results indicate that the Rh−pyridyl axial coordination bond in $\mathbf{1}_4$•**4a** is extremely strong and that $\mathbf{1}_4$•**4a** is thermodynamically stable even at 358 K[8,15,16] although rotation about the C−C bond between the porphyrin ring and the *p*-tolyl group becomes fast on the NMR time scale above 348 K. In fact, under the conditions of [**1**] = 6 mM and [**4a**] = 0.75 mM in $CDCl_3$, namely, [free **1**] = 3 mM and [$\mathbf{1}_4$•**4a**] = 0.75 mM (subunit-**1** in $\mathbf{1}_4$•**4a** is equivalent to 3 mM), the 2D NOESY spectrum showed no exchange cross-peaks between $\mathbf{1}_4$•**4a** and free **1** even at 323 K (Figure S12). This result indicates that the dissociation rate of the Rh−pyridyl axial coordination bond in $\mathbf{1}_4$•**4a** is too slow and below the detection limits on the NMR time scale.[15]

Figure 2 shows the UV−vis absorption spectra of $\mathbf{1}_4$•**4a** ([**1**] = 3.6 × 10^{-5} M and [**4a**] = 0.9 × 10^{-5} M) and **1** alone ([**1**] = 3.6 × 10^{-5} M) in toluene. The Soret band and Q-bands of $\mathbf{1}_4$•**4a** shifted to longer wavelengths with increases in their molar absorption coefficients, relative to those of free **1**. The spectral data are summarized in Table S1.

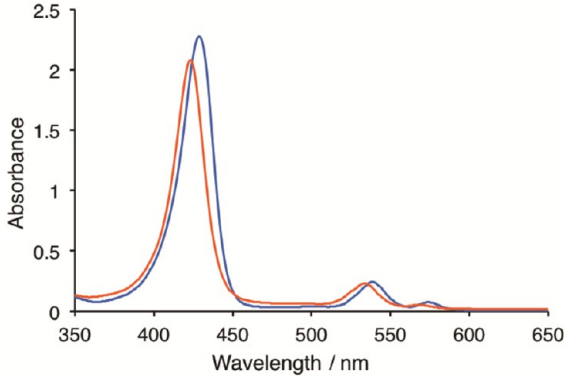

Figure 2. UV−vis absorption spectra of $\mathbf{1}_4$•**4a** (blue line: [**1**] = 3.6 × 10^{-5} M and [**4a**] = 0.9 × 10^{-5} M) and **1** alone (red line: [**1**] = 3.6 × 10^{-5} M) in toluene at 298 K.

X-ray Crystal Structure of $\mathbf{1}_4$•4b. Single crystals of $\mathbf{1}_4$•**4b**, suitable for X-ray diffraction analysis, were obtained by slow diffusion of EtOH into a $CHCl_3$ solution of a 4:1 mixture of **1** and **4b** (R = $CH_2CH(CH_3)_2$).[12b] An ORTEP view and crystal data are shown in Figure S13 and Table S2, respectively. The ^{1}H NMR spectrum of a solution of $\mathbf{1}_4$•**4b** upon dissolving the single crystals in CD_2Cl_2 showed that single crystals of $\mathbf{1}_4$•**4b** include EtOH and $CHCl_3$ as cocrystal solvents in a ratio of $\mathbf{1}_4$•**2b**/EtOH/$CHCl_3$ = 1:7:7 (Figure S14). Single-crystal X-ray diffraction analysis of $\mathbf{1}_4$•**4b** indicated chiral space group *I*4. The molecular structure of $\mathbf{1}_4$•**4b** in the single crystal is shown in Figure 3. Four molecules of achiral **1** and one molecule of **4b** self-assemble into $\mathbf{1}_4$•**4b** with a chiral arrangement of the assembling $\mathbf{1}_4$-unit through the Rh−pyridyl axial coordination bonds (Figure 3a−h), with the Rh−Npy atomic distance of 2.07 Å, the Cl−Rh−Npy angle of 177.4°, and the Rh−Npy··· C4py angle of 164.3° (Figure 3k).[4a] As shown in Figure 3a−d, $\mathbf{1}_4$•**4b** seems to be a quadruple interlocking gear. Four subunits-**1** are gear wheels, wherein the porphyrin ring is a rotor and the four protruding *p*-tolyl groups at the *meso*-positions are teeth. Four *p*-pyridyl groups in subunit-**4b**, i.e., the Rh−Py axial coordination bonds, are rotation axes of the gear wheels. In the assembling $\mathbf{1}_4$-unit shown in Figure 3e−h, two inwardly oriented *p*-tolyl groups shown in purple (A and B) of each subunit-**1** cruciately interdigitate with one of two inwardly oriented *p*-tolyl groups of two adjacent subunits-**1** at both sides to form four sets of cruciform π-stack dimers of *p*-tolyl groups (A1 and B2, A2 and B3, A3 and B4, and A4 and B1; see also Figure 5a,b). One of the two inwardly oriented *p*-tolyl groups (A) of each subunit-**1** is regularly placed at the inside position of the π-stack dimer of the *p*-tolyl groups, and the other of the two inwardly oriented *p*-tolyl groups (B) of each subunit-**1** is regularly placed at the outside position of the π-stack dimer. In other words, one subunit-**1** and two adjacent subunits-**1** at both sides interlock with one another cooperatively. Thus, the top

DOI: 10.1021/jacs.6b07284
J. Am. Chem. Soc. 2016, 138, 12564−12577

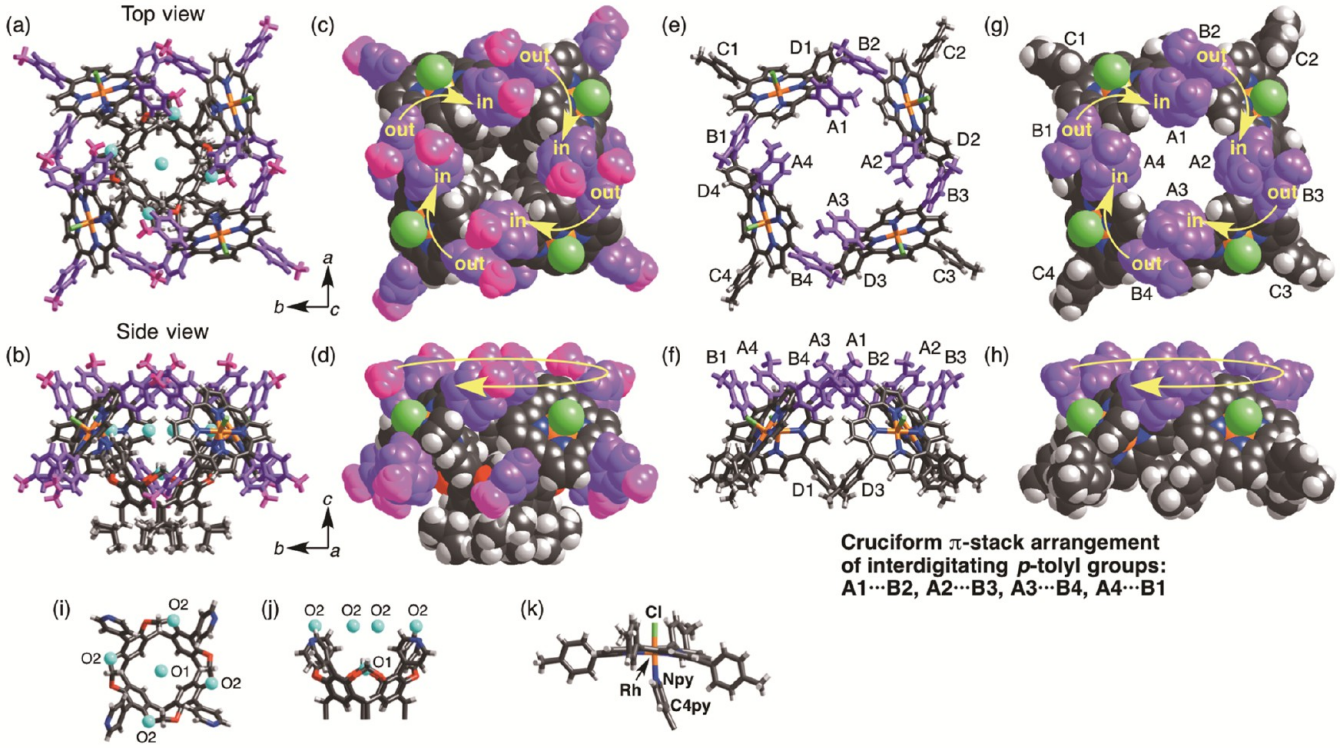

Figure 3. Molecular structure of $\mathbf{1}_4$•**4b** in the X-ray crystal structure: (a and c) top view (viewed down the *c*-axis) and (b and d) side view (viewed down the *a*-axis), wherein the CH_3 group and the C_6H_4 ring of the *p*-tolyl groups of each subunit-**1** are highlighted as red purple and purple, respectively. In a and b, the oxygen atoms of the encapsulated EtOH molecules are shown in light blue. Assembling $\mathbf{1}_4$-unit in $\mathbf{1}_4$•**4b**: (e and g) top view and (f and h) side view, wherein two inwardly oriented *p*-tolyl groups of each subunit-**1** are highlighted as purple and subunit-**4b** is omitted for clarity. Subunit-**4b** with the encapsulated EtOH molecules: (i) top view and (j) side view, wherein EtOH molecules are heavily disordered and only oxygen atoms are shown in light blue for clarity (occupancy factor: O1 = 1, O2 = 0.5). The side chains of subunit-**4b** are replaced by carbon atoms for clarity. (k) Subunit-**1** with axial coordination of the pyridyl moiety of subunit-**4b**.

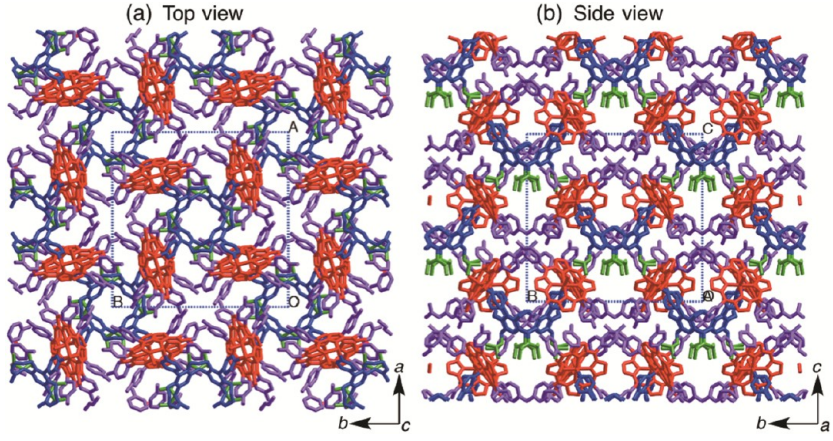

Figure 4. 3D packing structure of $\mathbf{1}_4$•**4b** in the X-ray crystal structure: (a) top view (viewed down the *c*-axis) and (b) side view (viewed down the *a*-axis). The porphyrin ring and the *p*-tolyl groups of each subunit-**1** are shown in red and purple, respectively, and the cavitand and its side chains of subunit-**4b** are shown in blue and green, respectively. Hydrogen atoms of $\mathbf{1}_4$•**4b** and cocrystal solvents (EtOH and $CHCl_3$) are omitted for clarity.

view (view down along the *c*-axis) of $\mathbf{1}_4$•**4b** indicates that the assembling $\mathbf{1}_4$-unit is oriented clockwise, as shown in Figure 3a,c,e,g. Therefore, the regular interdigitation of inwardly oriented *p*-tolyl groups of the four achiral subunits-**1** forms the arrangement of the assembling $\mathbf{1}_4$-unit chiral.

Figure 4 shows the 3D packing structure of $\mathbf{1}_4$•**4b** in the X-ray crystal structure. The top view (view down along the *c*-axis) indicates that all assembling $\mathbf{1}_4$-units in the crystal of $\mathbf{1}_4$•**4b** are arranged in the same clockwise orientation. Furthermore, a side view (view along the *a*-axis) indicates that all $\mathbf{1}_4$•**4b** are unidirectionally aligned along the *c*-axis. Thus, the single crystal of $\mathbf{1}_4$•**4b** self-assembled by achiral **1** and **4b** gave chiral space group *I*4.[17−19]

As shown in Figure 3, $\mathbf{1}_4$•**4b** possesses an entrance aperture for guest encapsulation with diameter of 6.7 Å at a maximum including van der Waals radii and an inner space in which at least three molecules of EtOH can be encapsulated (Figures 3a,b,i,j), although EtOH and $CHCl_3$ molecules as cocrystal solvents were highly disordered. The N···N atomic distances between two *p*-pyridyl groups at the adjacent and diagonal

DOI: 10.1021/jacs.6b07284
J. Am. Chem. Soc. 2016, 138, 12564−12577

positions of subunit-**4b** in $\mathbf{1}_4$•**4b** were 9.7 and 13.7 Å, respectively, the values of which are 1.0 and 1.4 Å, respectively, greater than those of the calculated structure of **4** as mentioned above, probably because of the steric congestion between the adjacent subunits-**1**.

Dynamic Behavior of $\mathbf{1}_4$•4a in Solution as a Quadruple Interlocking Gear. As mentioned above, the following three features are noteworthy concerning the structural properties of $\mathbf{1}_4$•**4a** and $\mathbf{1}_4$•**4b**: (i) extremely strong porphyrin-Rh−pyridyl axial coordination bond, revealed by the NMR studies of $\mathbf{1}_4$•**4a** at 298−358 K (Figures S10 and S12),[8,15] (ii) rigidity of the methylene-bridge cavitand as a scaffold of the pyridyl axes,[12] and (iii) cruciform arrangement of four sets of the interdigitating *p*-tolyl groups as the teeth moiety of the gear wheels in the assembling $\mathbf{1}_4$-unit, revealed by the X-ray crystallographic analysis of $\mathbf{1}_4$•**4b** (Figures 3 and 5a−c).

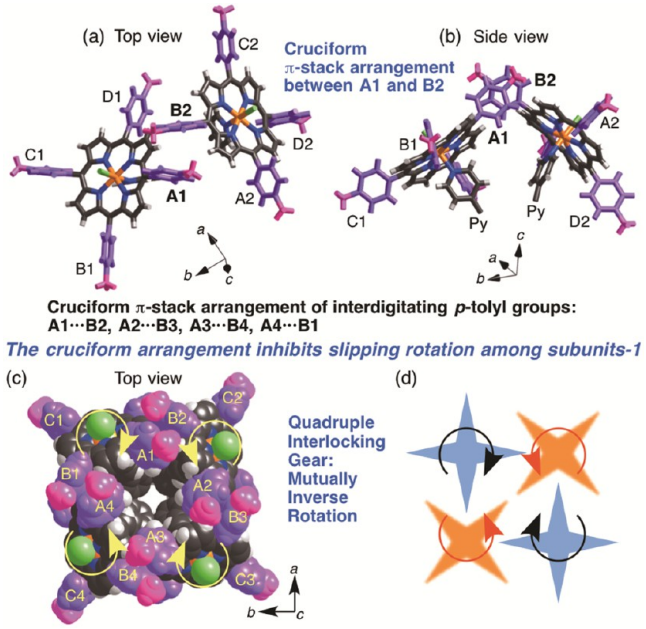

Figure 5. Cruciform arrangement of the interdigitating *p*-tolyl groups A1 and B2 between adjacent two subunits-**1** in $\mathbf{1}_4$•**4b** in the X-ray crystal structure: (a) top view and (b) side view. (c) $\mathbf{1}_4$•**4b** in the X-ray crystal structure. (d) Schematic representation of interlocking gear of four subunits-**1** in $\mathbf{1}_4$•**4**.

Judging from these results in a comprehensive manner, it is strongly suggested that $\mathbf{1}_4$•**4a** in solution behaves as a quadruple interlocking gear, wherein one subunit-**1** and two adjacent subunits-**1** interlock cooperatively, with mutually inverse rotation (Figure 5d). The strong bond excludes a dissociation−association mechanism of the Rh−pyridyl coordination bond in $\mathbf{1}_4$•**4a** for random rotation. Based on the rigidity and cruciform arrangement, a slipping rotation between adjacent subunits-**1** with the cruciately interdigitating *p*-tolyl groups would be sterically impossible in $\mathbf{1}_4$•**4a**, without relation to rotation about the C−C bond between the porphyrin ring and the *p*-tolyl group. In addition, the Rh−Npy···C4py angle in $\mathbf{1}_4$•**4b** was 164.3° (Figure 3k),[4a] suggesting that the Rh−pyridyl coordination bond in $\mathbf{1}_4$•**4a** is unlikely to be bent more than this angle for a slipping rotation between adjacent subunits-**1**. Thus, it is strongly suggested that $\mathbf{1}_4$•**4a** in solution behaves as a quadruple interlocking gear. The results of activation parameters ($\Delta H^{\ddagger}$, $\Delta S^{\ddagger}$, and $\Delta G^{\ddagger}$) obtained from Eyring plots based on line-shape analysis of the VT ^{1}H NMR spectra of $\mathbf{1}_4$•**4a** also support the interlocking rotation (geared coupled motion) mechanism (vide infra).

If the interlocking rotation of four subunits-**1** is slow on the NMR time scale, then each subunit-**1** would be desymmetrized and the ^{1}H NMR signals of the pyrrole-*β*H and the CH_3 group of the *p*-tolyl group in subunit-**1** would appear as up to 8 and 4 sets of signals, respectively.[8] In contrast, if the interlocking rotation of the four subunits-**1** is faster than the NMR time scale, then each subunit-**1** would be symmetrized as an averaged form and the ^{1}H NMR signals of the pyrrole-*β*H and the CH_3 group of the *p*-tolyl group would appear as one singlet signal.[8] The signals of the aryl-A−D protons of the *p*-tolyl groups in subunit-**1** would also behave in a similar way to that of the CH_3 group of the *p*-tolyl group (up to 16 sets of signals). As noted above (Figure 1b), the ^{1}H NMR spectrum of $\mathbf{1}_4$•**4a** in $CDCl_3$ at 298 K showed, respectively, one singlet signal of the pyrrole-*β*H (F) and the CH_3 group (E) of the *p*-tolyl group in subunit-**1** as an averaged form and indicated the faster rotation of the four subunits-**1** than the NMR time scale.

Figure 6 shows VT ^{1}H NMR spectra of $\mathbf{1}_4$•**4a** in CD_2Cl_2 at 298−188 K. The singlet signal of the pyrrole-*β*Hs (F) and the CH_3 groups (E) of the *p*-tolyl groups in subunit-**1** became broadened at 238 K and began to split at 218−208 K. The signals of the aryl-C and -D protons on the Rh−pyridyl side and the signals of the aryl-A and -B protons on the Rh−Cl side of the *p*-tolyl groups in subunit-**1** became broadened at 238 and 218 K, respectively. The former would be more sensitive to geared motion than the latter probably because of proximity effect of subunit-**4a**. Furthermore, the signals of the C and D protons were coalesced at 218 K.

These results strongly suggest that $\mathbf{1}_4$•**4a** behaves as a quadruple interlocking gear and that the interlocking rotation of the four subunits-**1** in $\mathbf{1}_4$•**4a** becomes slow on the NMR time scale below 218−208 K. Furthermore, the gear function of $\mathbf{1}_4$•**4a** was also supported by the rotation behaviors of the following 4:1 complexes based on the combinations of Rh(III)Cl *meso*-tetraarylporphyrins bearing various teeth-moiety and tetra(*p*-pyridyl)cavitand derivatives: $\mathbf{2}_4$•**4a**, $\mathbf{3a}_4$•**4a**, $\mathbf{3b}_4$•**4a**, and $\mathbf{1}_4$•**5**.

Formation and Dynamic Behavior of $\mathbf{2}_4$•4a in Solution as a Quadruple Interlocking Gear. First, the combination of **4a** and *meso*-tetrakis[4-(4-methylphenyl)-phenyl]porphyrinato Rh(III)Cl **2** is a tooth-expanded version of **1** as a gear wheel (Scheme 2). Based on the X-ray crystal structure of $\mathbf{1}_4$•**4b** (Figure 5), it is expected that replacement of the *p*-tolyl group in **1** by the *p*-methylbiphenyl group in **2** would not block the formation of $\mathbf{2}_4$•**4a** because of protrusion of the additional *p*-tolyl groups on the cruciform arrangement of the interdigitating *p*-tolyl groups in subunits-**1**. In fact, in a way similar to that of $\mathbf{1}_4$•**4a**, a 4:1 mixture of **2** and **4a** quantitatively self-assembled into $\mathbf{2}_4$•**4a** as a highly symmetrical single species in $CDCl_3$ at 298 K (Figures 7b and S15), wherein the $\Delta\delta$ values of the ^{1}H NMR signals of the Py*α*-proton (a) and Py*β*-proton (b) of subunit-**4a** were ca. −7.69 and −2.75 ppm, respectively.[20] The ^{1}H NMR spectrum of $\mathbf{2}_4$•**4a** in $CDCl_3$ at 298 K showed, respectively, one singlet signal of the pyrrole-*β*H (H) and the CH_3 group (G) of the *p*-methylbiphenyl group in the subunit-**2** as an averaged form. This result indicates the rotation of four subunits-**2** was faster than the NMR time scale at 298 K, although these two signals of $\mathbf{2}_4$•**4a** were somewhat broadened compared with those of $\mathbf{1}_4$•**4a**.

DOI: 10.1021/jacs.6b07284
J. Am. Chem. Soc. 2016, 138, 12564−12577

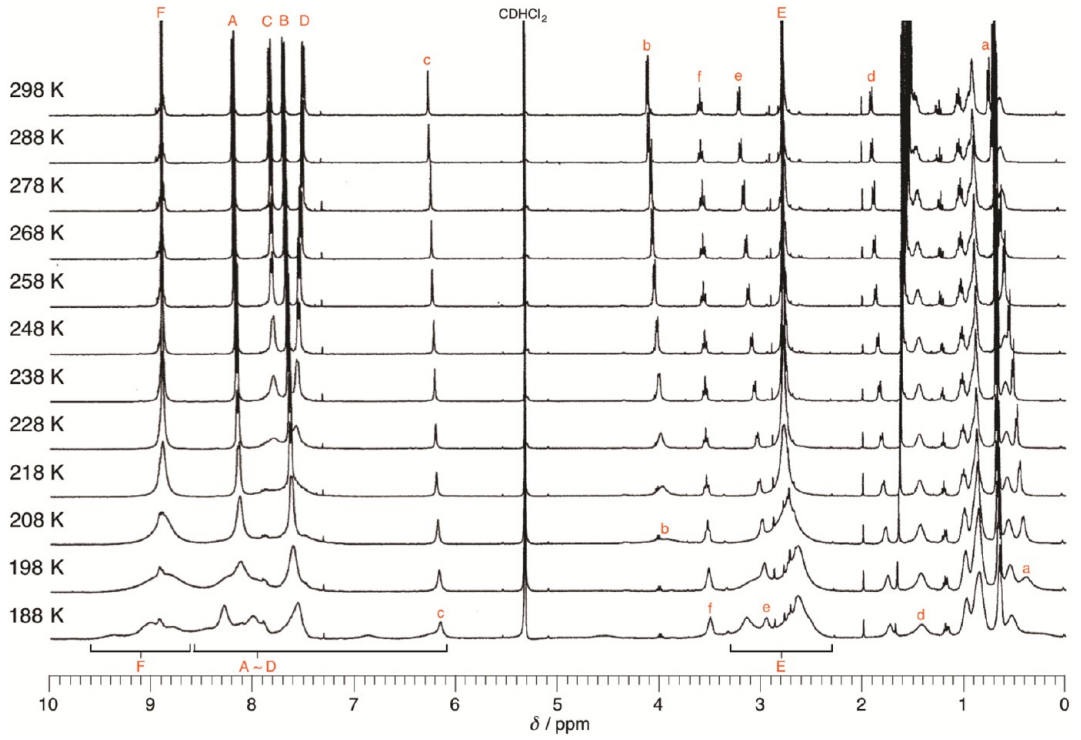

Figure 6. Temperature dependence of the ^{1}H NMR spectra (400 MHz) of $\mathbf{1}_4$•**4a** (2 mM) in CD_2Cl_2 at 298−188 K.

Scheme 2. Self-Assembly of a 4:1 Mixture of 2 and 4a into $\mathbf{2}_4$•4a through Rh−Pyridyl Axial Coordination Bonds

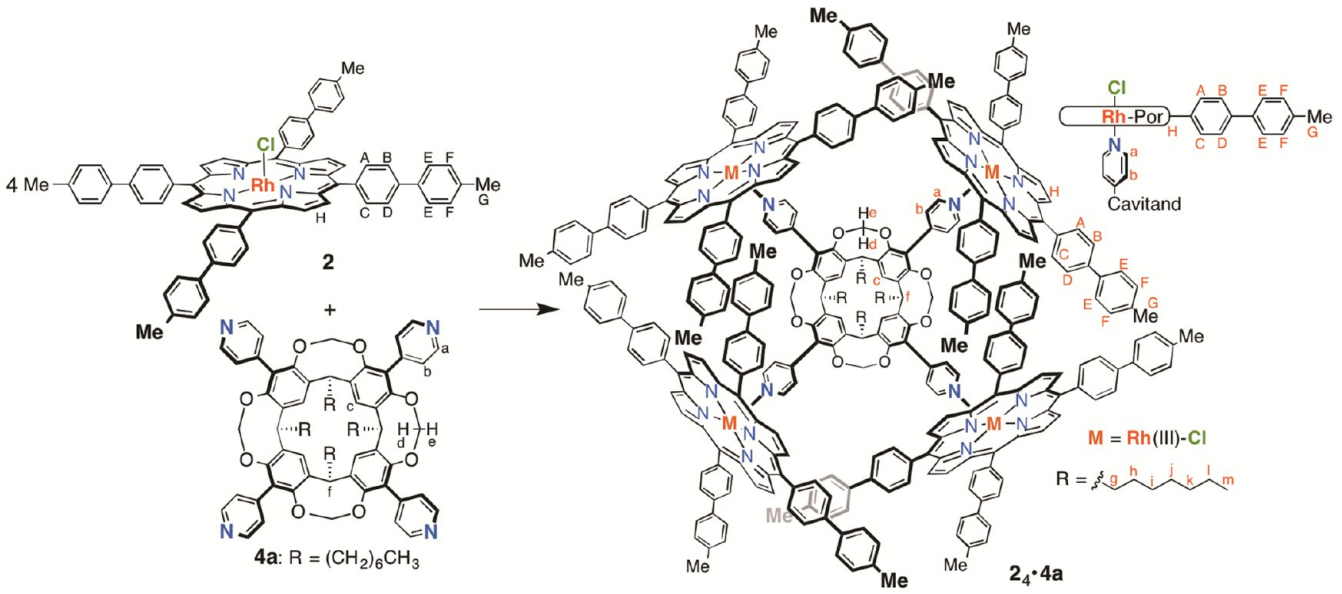

Figure 8 shows VT ^{1}H NMR spectra of $\mathbf{2}_4$•**4a** in CD_2Cl_2 at 298−188 K. The singlet signal of the pyrrole-βHs (H) and the CH_3 group (G) of the *p*-methylbiphenyl groups in subunit-**2** became broadened at 228 K but did not split even at 188 K. In $\mathbf{2}_4$•**4a**, a slipping rotation between adjacent subunits-**2** with the cruciately interdigitating *p*-methylbiphenyl groups as a tooth-expanded version of **1** is absolutely impossible. These results indicate that $\mathbf{2}_4$•**4a** behaves as a quadruple interlocking gear and suggest that it is hard to stop the interlocking rotation of the assembling $\mathbf{2}_4$-unit in $\mathbf{2}_4$•**4a** with longer teeth compared with that of the assembling $\mathbf{1}_4$-unit in $\mathbf{1}_4$•**4a** with shorter teeth. A possible reason for this behavior may be related to the activation parameters for the interlocking rotation (vide infra).

Formation and Dynamic Behavior of $\mathbf{3a}_4$•4a in Solution as a Quadruple Interlocking Gear. Second, the combination of **4a** and *meso*-tetrakis(3,5-dimethoxyphenyl)-porphyrinato Rh(III)Cl **3a** is another version of teeth-moiety of **1** (Scheme 3). In a way similar to that of $\mathbf{1}_4$•**4a**, a 4:1 mixture of **3a** and **4a** quantitatively self-assembled into $\mathbf{3a}_4$•**4a** as a highly symmetrical single species in $CDCl_3$ at 298 K (Figures S16−S18), wherein the $\Delta\delta$ values of the ^{1}H NMR signals of the Pyα-proton (a) and Pyβ-proton (b) of subunit-**4a** were −7.79 and −2.78 ppm, respectively. The signal of the pyrrole-βH (signal

DOI: 10.1021/jacs.6b07284
J. Am. Chem. Soc. 2016, 138, 12564−12577

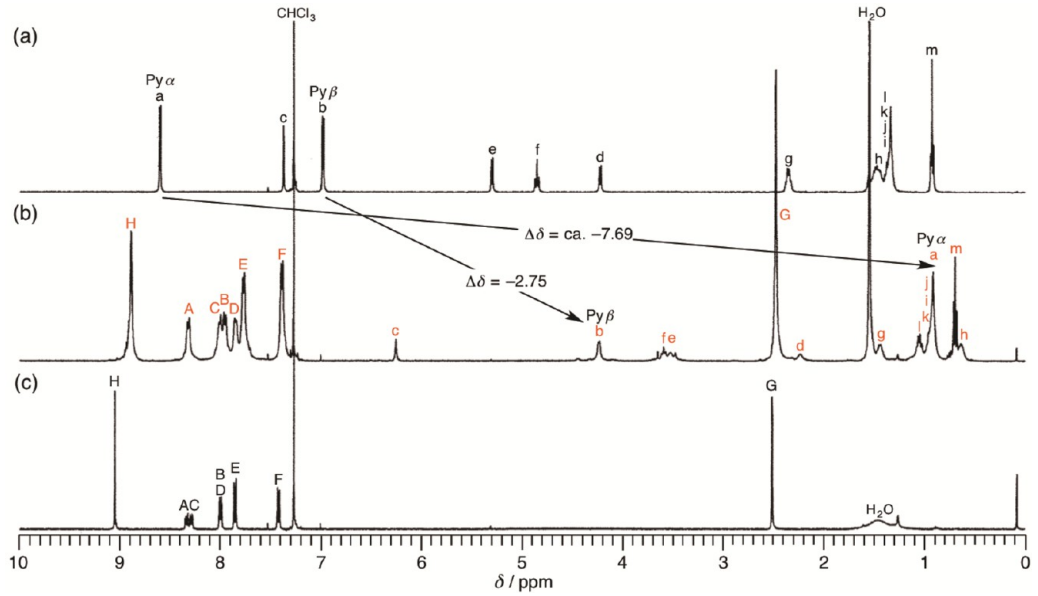

Figure 7. ^{1}H NMR spectra (400 MHz, $CDCl_3$, 298 K): (a) **4a** alone, (b) **2**$_4$•**4a** ([**2**] = 4 mM and [**4a**] = 1 mM), and (c) **2** alone. The signals marked "A−H" and "a−m" are assigned in Scheme 2.

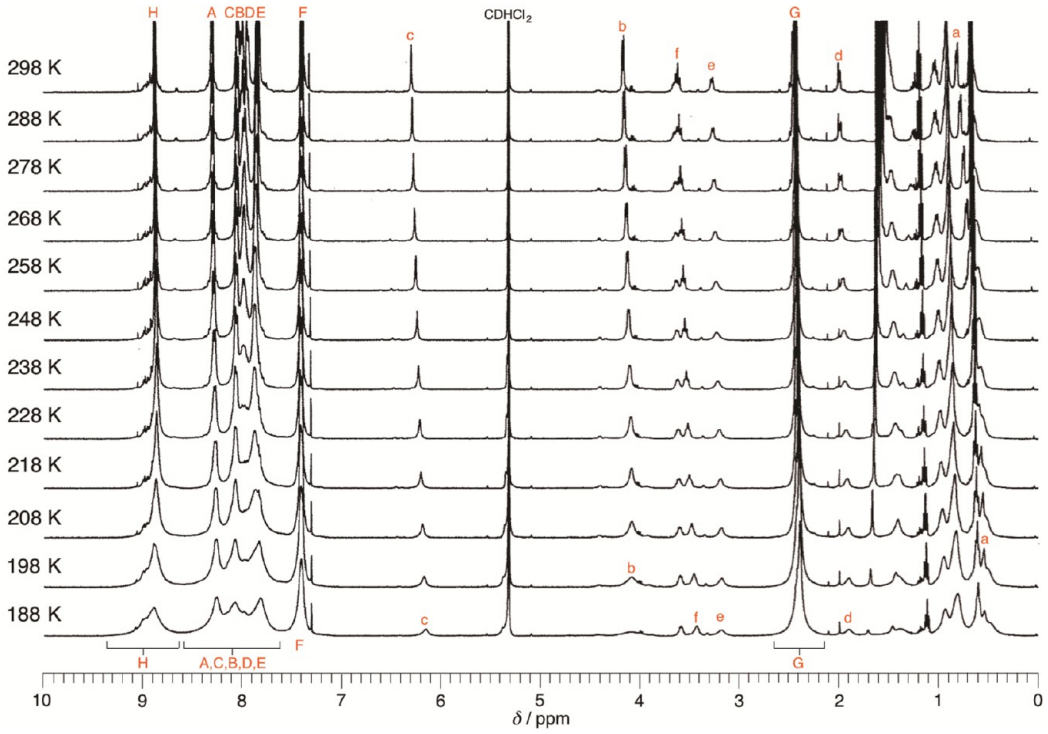

Figure 8. Temperature dependence of the ^{1}H NMR spectra (400 MHz) of **2**$_4$•**4a** (1 mM) in CD_2Cl_2 at 298−188 K.

F) of subunit-**3a** appeared as one singlet signal as an averaged form. These results indicate that the rotation of the four subunits-**3a** in **3a**$_4$•**4a** was faster than the NMR time scale at 298 K.

Figure 9 shows VT ^{1}H NMR spectra of **3a**$_4$•**4a** in CD_2Cl_2 at 298−188 K. The singlet signal of the pyrrole-*β*Hs (F) and the *p*-protons (E) of the 3,5-dimethoxyphenyl groups in subunit-**3a** became broadened at 238 K and highly broadened at 218−208 K but did not split even at 188 K. The signals of the aryl-C and methoxy-D protons on the Rh−pyridyl side and the signals of the aryl-A and methoxy-B protons on the Rh−Cl side of the 3,5-dimethoxyphenyl groups in subunit-**3a** became broadened at 248 and 218 K, respectively. Furthermore, the signals C and D became highly broadened at 228 K and almost disappeared at 208 K.

Formation and Dynamic Behavior of 3b$_4$•4a in Solution as a Quadruple Interlocking Gear. Third, the combination of **4a** and *meso*-tetrakis(3,5-di-*n*-propoxyphenyl)-porphyrinato Rh(III)Cl **3b** is a sterically bulky version of **3a** and **1** (Scheme 4). A 4:1 mixture of **3b** and **4a** quantitatively self-assembled into **3b**$_4$•**4a** as a highly symmetrical single species in $CDCl_3$ at 298 K (Figures 10b, S19, and S20),

DOI: 10.1021/jacs.6b07284
J. Am. Chem. Soc. 2016, 138, 12564−12577

Scheme 3. Self-Assembly of a 4:1 Mixture of 3a and 4a into $3a_4$•4a through Rh−Pyridyl Axial Coordination Bonds

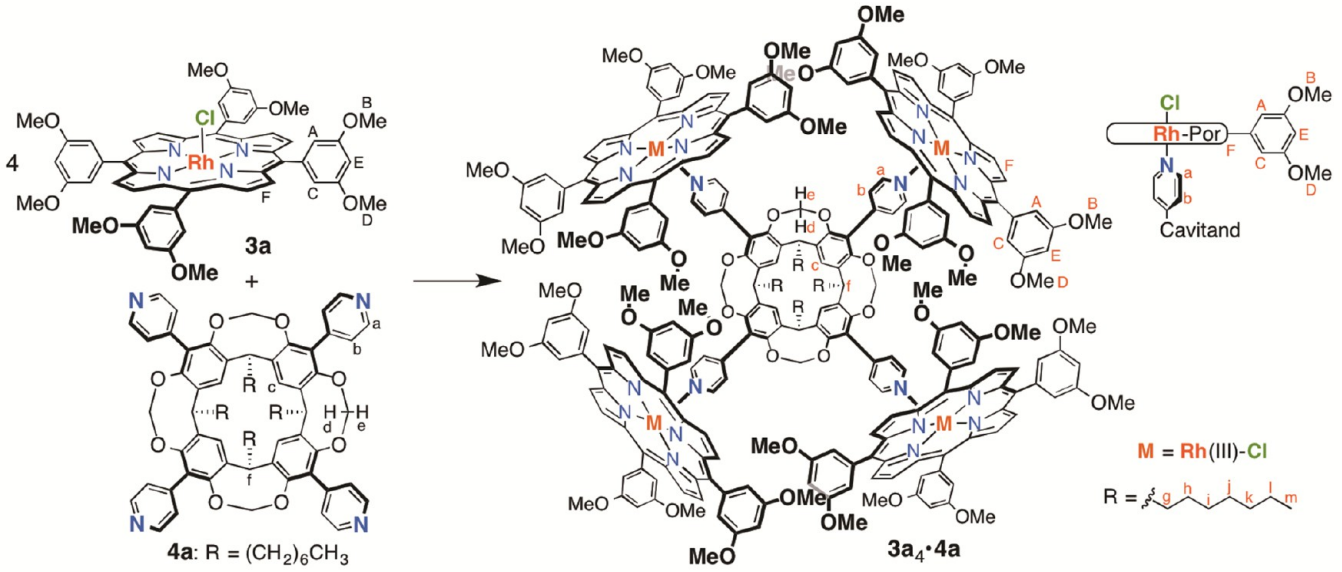

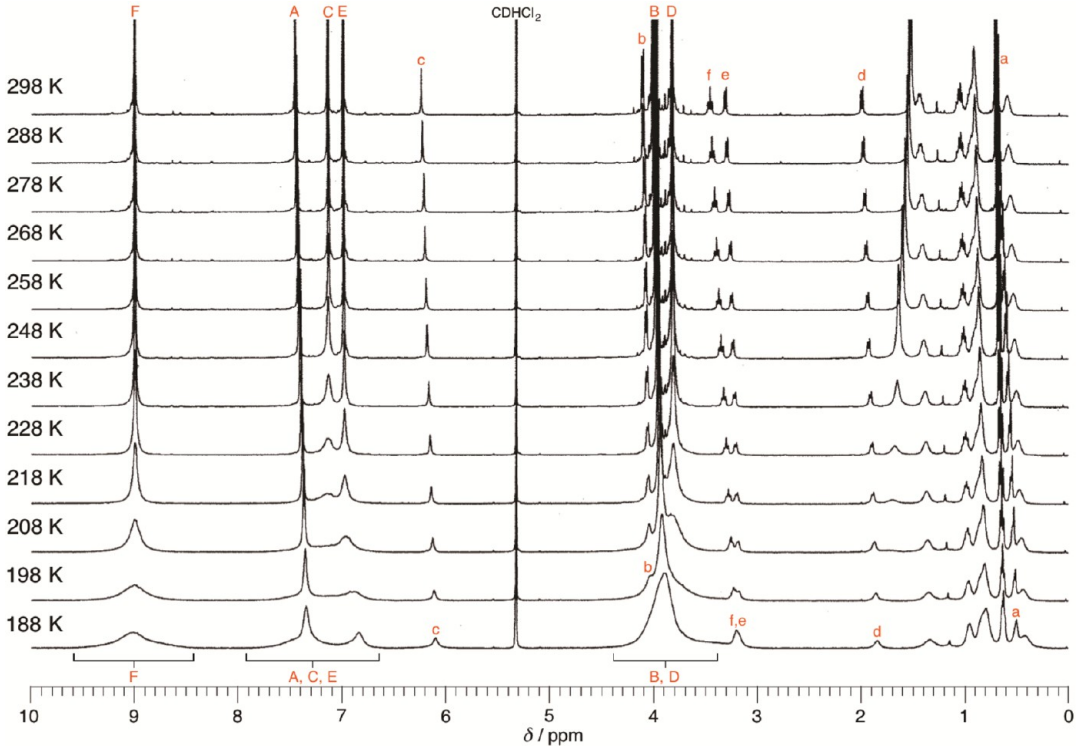

Figure 9. Temperature dependence of the ^{1}H NMR spectra (400 MHz) of $3a_4$•4a (2 mM) in CD_2Cl_2 at 298−188 K.

although the assembling $3b_4$-unit is sterically more congested than the assembling $3a_4$-unit and 1_4-unit. The $\Delta\delta$ values of the ^{1}H NMR signals of the Pyα-proton (a) and Pyβ-proton (b) of subunit-**4a** in $3b_4$•**4a** were −7.86 and −2.87 ppm, respectively.[21] In a way similar to that of $3a_4$•**4a**, rotation about the C−C bond between the porphyrin ring and the 3,5-di-*n*-propoxyphenyl group in $3b_4$•**4a** was slow on the NMR time scale at 298 K, leading to the appearance of two singlet signals of the *o*-protons (signals A and C) and two sets of signals of the *m*-*n*-propoxy groups (B, F, and G; D, F′, and G′) of the 3,5-di-*n*-propoxyphenyl group, wherein signals A, B, F, and G are on the Rh−Cl side and signals C, D, F′, and G′ are on the Rh−pyridyl side. The signal of the pyrrole-βH (signal H) of subunit-**3b** appeared as one singlet signal as an averaged form. These results indicate that the rotation of the four subunits-**3b** in $3b_4$•**4a** was faster than the NMR time scale at 298 K. A slipping rotation between adjacent subunits-**3b** with the cruciately interdigitating 3,5-di-*n*-propoxyphenyl groups is also sterically impossible in $3b_4$•**4a**.

VT ^{1}H NMR spectra of $3b_4$•**4a** in $CDCl_2CDCl_2$ at 298−358 K are shown in Figure S21, wherein all signals and their chemical shifts almost remained unchanged even at 358 K. This result indicates that the Rh−pyridyl axial coordination bond in $3b_4$•**4a** is also extremely strong and that $3b_4$•**4a** is

DOI: 10.1021/jacs.6b07284
J. Am. Chem. Soc. 2016, 138, 12564−12577

Scheme 4. Self-Assembly of a 4:1 Mixture of 3b and 4a into $3b_4$•4a through Rh−Pyridyl Axial Coordination Bonds

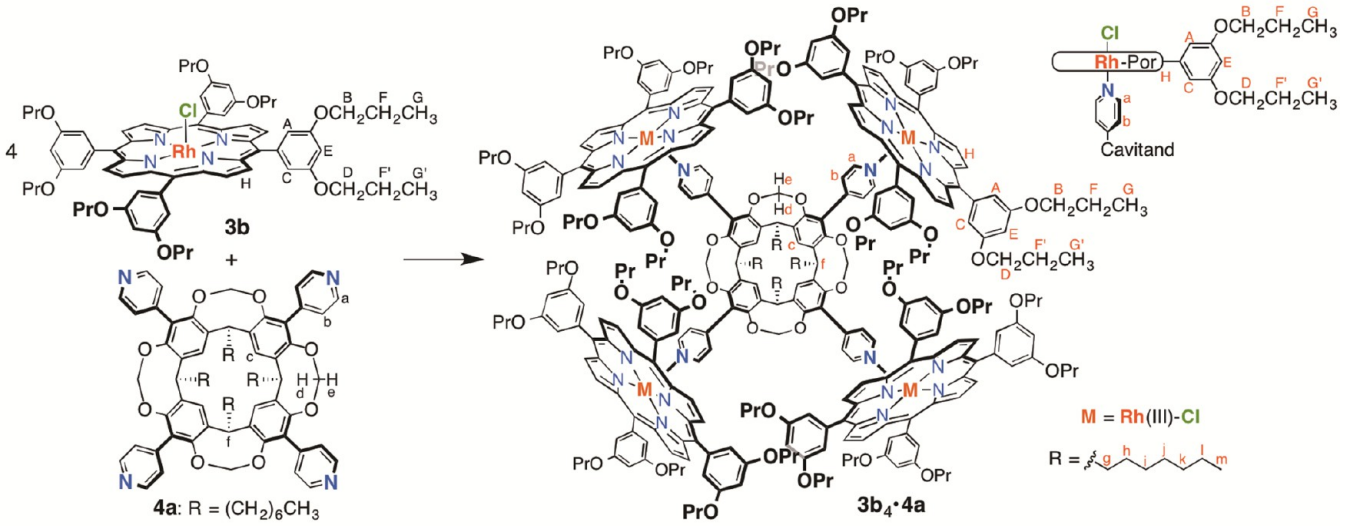

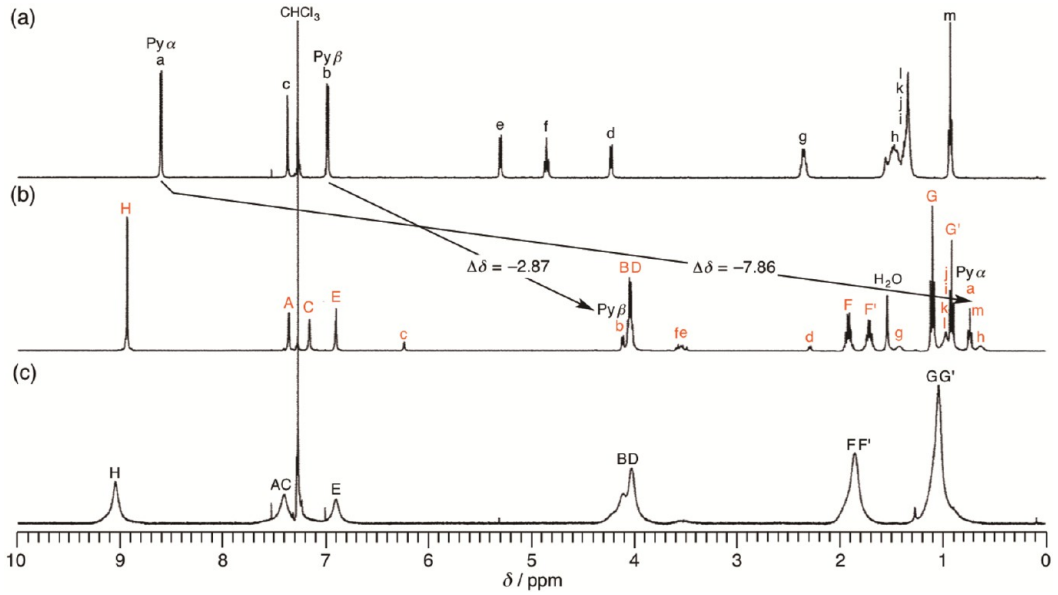

Figure 10. ^{1}H NMR spectra (400 MHz, $CDCl_3$, 298 K): (a) **4a** alone, (b) **$3b_4$•4a** ([**3b**] = 8 mM and [**4a**] = 2 mM), and (c) **3b** alone. The signals marked "A−H" and "a−m" are assigned in Scheme 4.

thermodynamically stable even at 358 K. This result also indicates that rotation about the C−C bond between the porphyrin ring and the 3,5-di-*n*-propoxyphenyl group in **$3b_4$•4a** is slow on the NMR time scale even at 358 K.

Figures 11 and S22 show VT ^{1}H NMR spectra of **$3b_4$•4a** in CD_2Cl_2 at 298−188 K. At a lower temperature, the signal changes of **$3b_4$•4a** were more noticeable than those of **$3a_4$•4a**. The singlet signal of the pyrrole-*β*Hs (H) and the *p*-protons (E) of the 3,5-di-*n*-propoxyphenyl groups in subunit-**3b** became broadened at 248 K and began to split at 228 K. The signal of the *o*-protons (C) on the Rh−pyridyl side and the *o*-protons (A) on the Rh−Cl side of the 3,5-di-*n*-propoxyphenyl groups in subunit-**3b** became broadened at 278 and 238 K, respectively. Furthermore, signal C disappeared at 238 K, and signal A became highly broadened at 218 K. Finally, at 188 K, the signal of the pyrrole-*β*Hs (H) split into 7 sets of signals, and the signals of the aryl-A, -C, and -E protons split into 9−10 sets of signals in total. When the interlocking rotation of four subunits-**3b** is very slow on the NMR time scale, each subunit-**3b** in **$3b_4$•4a** is desymmetrized, leading to the appearance of up to 8 sets of the ^{1}H NMR signals of the pyrrole-*β*Hs and up to 12 sets of the signals of the aryl-A, -C, and -E protons in total (3 × 4 sets). These results clearly indicate that **$3b_4$•4a** behaves as a quadruple interlocking gear and that the interlocking rotation (geared coupled motion) of the four subunits-**3b** in **$3b_4$•4a** becomes slow on the NMR time scale below 238−228 K.

Formation and Dynamic Behavior of 1_4•5 in Solution. Fourth, the combination of **1** and tetrakis[4-(4-pyridyl)-phenyl]cavitand **5** (R = $(CH_2)_6CH_3$) is an axis-expanded version of **4a** (Scheme 5). A 4:1 mixture of **1** and **5** quantitatively self-assembled into **1_4•5** in $CDCl_3$ at 298 K (Figures S23 and S24), wherein the $\Delta\delta$ values of the ^{1}H NMR signals of the Py*α*-proton (a) and Py*β*-proton (b) of subunit-**5** were −7.65 and −2.41 ppm, respectively. In marked contrast to **1_4•4a**, **2_4•4a**, **$3a_4$•4a**, and **$3b_4$•4a**, VT ^{1}H NMR spectra of **1_4•5** in CD_2Cl_2 at 298−188 K showed that the singlet signal of

DOI: 10.1021/jacs.6b07284
J. Am. Chem. Soc. 2016, 138, 12564−12577

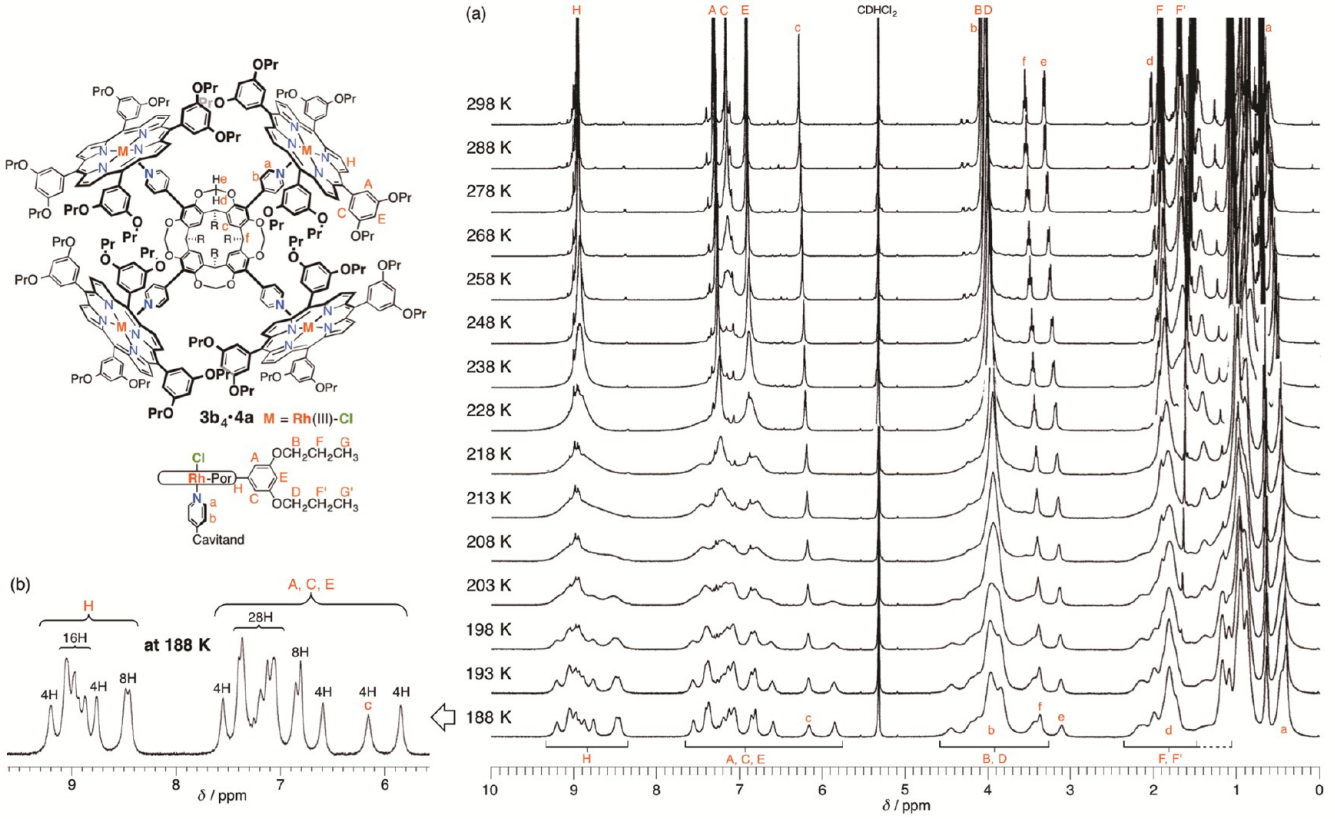

Figure 11. (a) Temperature dependence of the ^{1}H NMR spectra (400 MHz) of **3b$_4$•4a** (2 mM) in CD_2Cl_2 at 298−188 K and (b) expansion spectrum in the aromatic region at 188 K.

Scheme 5. Self-Assembly of a 4:1 Mixture of 1 and 5 into 1$_4$•5 through Rh−Pyridyl Axial Coordination Bonds

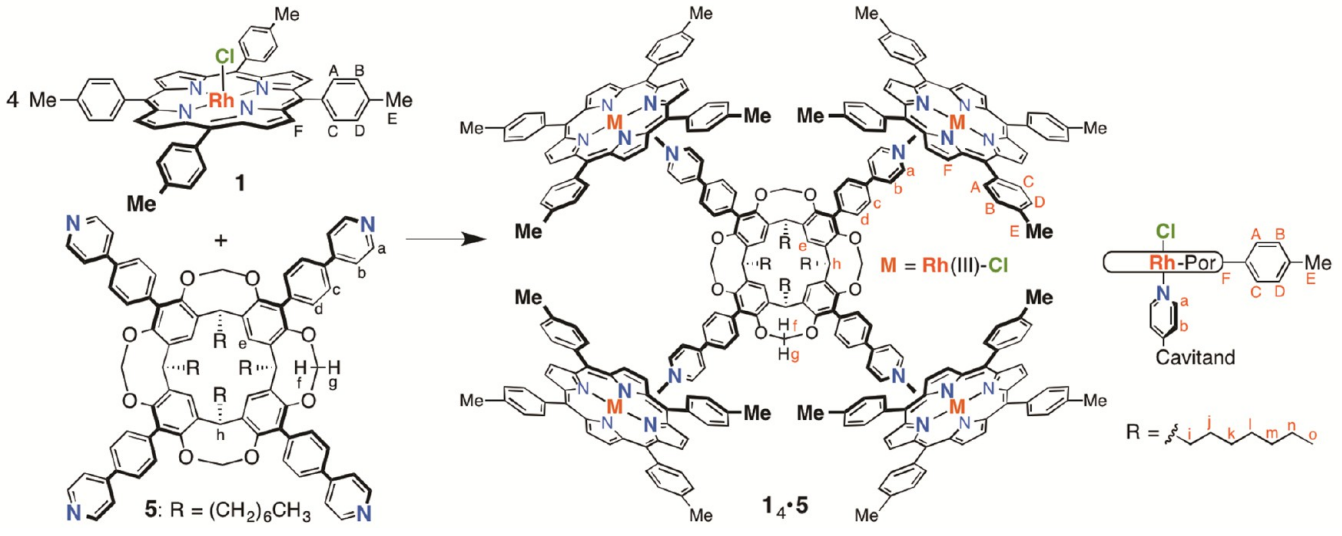

the pyrrole-βH (F) and the CH_3 group (E) of the *p*-tolyl group as well as the signals of the aryl-A−D protons of the *p*-tolyl group in subunit-**1**, remained completely unchanged even at 188 K (Figure 12). These results clearly indicate that the four subunits-**1** in **1$_4$•5** do not interlock with one another and randomly and freely rotate faster than the NMR time scale even at 188 K because the four *p*-(*p*-pyridyl)phenyl groups in subunit-**5** are too long to serve as axes of gear wheels. Thus, **1$_4$•5** did not behave as a gear.

Line-Shape Analysis of VT ^{1}H NMR Spectra: Activation Parameters of Quadruple Interlocking Gears. To obtain a deeper understanding of the present rotation characteristics, we performed the line-shape analysis of the VT ^{1}H NMR spectra using coupled stochastic Liouville equations for **1$_4$•4a**, **2$_4$•4a**, **3a$_4$•4a**, and **3b$_4$•4a** based upon the chemical shifts of the desymmetrized 8 sets (Figure 13b and Table S3) by the pyrrole-βHs, as detailed in the Supporting Information. Evaluations of the activation parameters from Eyring plots of exchange rates (k) between magnetic environments of 1 ⇄ 3, 1

DOI: 10.1021/jacs.6b07284
J. Am. Chem. Soc. 2016, 138, 12564−12577

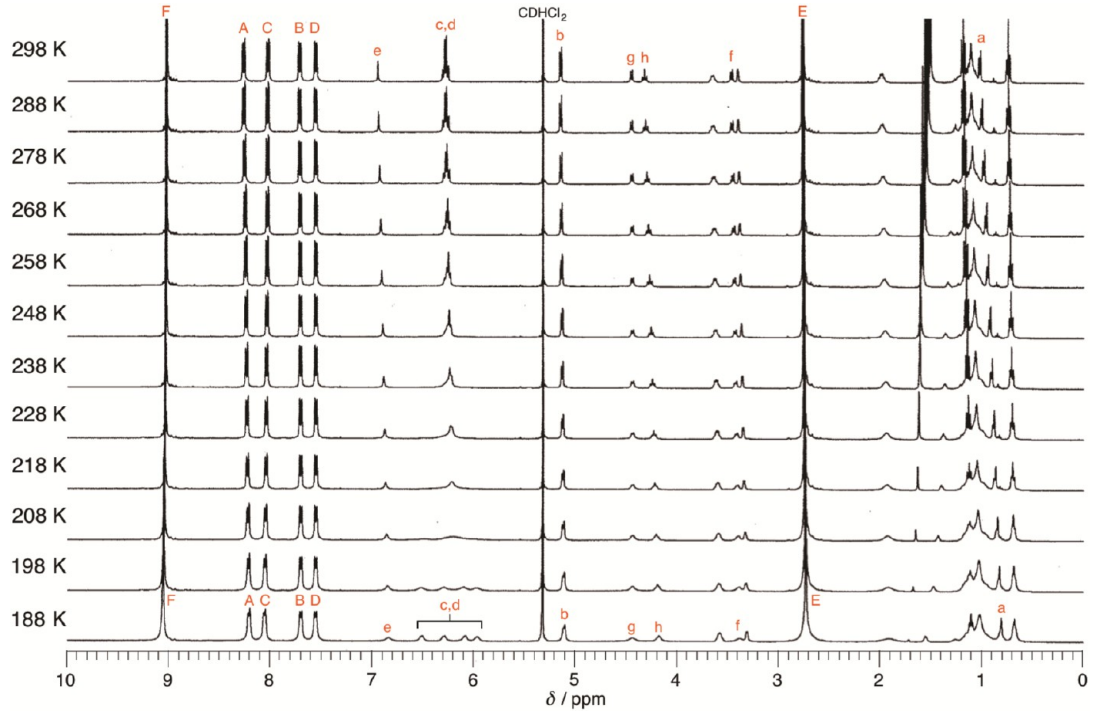

Figure 12. Temperature dependence of the ^{1}H NMR spectra (400 MHz) of $\mathbf{1}_4$•**5** (2 mM) in CD_2Cl_2 at 298−188 K.

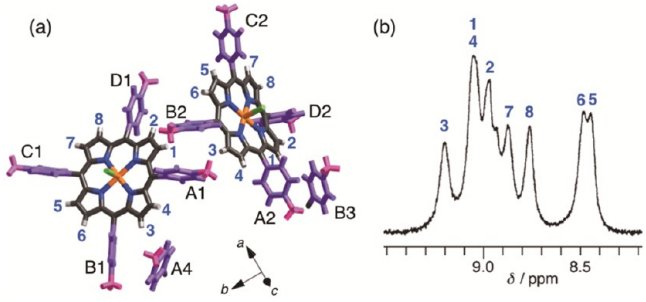

Figure 13. (a) Rotational model of the four RhCl-tetraarylporphyrin subunits in (RhCl-tetraarylporphyrin)$_4$•**4a** for the line-shape analysis of the VT ^{1}H NMR signals of the pyrrole-βHs based on the X-ray crystal structure of $\mathbf{1}_4$•**4b** and (b) the assignments of the 8 sets of the pyrrole-βH signals of $\mathbf{3b}_4$•**4a** in CD_2Cl_2 at 188 K deduced from the model.

⇄ 8, 2 ⇄ 4, 2 ⇄ 7, 3 ⇄ 5, 4 ⇄ 6, 5 ⇄ 8, and 6 ⇄ 7 in Figure 13a would give an insight into the rotational mechanism (geared coupled rotation or slipping rotation) of the four RhCl-tetraarylporphyrin subunits about the respective Rh−pyridyl axial coordination bond in $\mathbf{1}_4$•**4a**, $\mathbf{2}_4$•**4a**, $\mathbf{3a}_4$•**4a**, and $\mathbf{3b}_4$•**4a**.

As a typical example, Figure 14 shows the VT ^{1}H NMR signals of the pyrrole-βHs of $\mathbf{3b}_4$•**4a** in CD_2Cl_2 and their line-shape simulation, by which the exchange rate constants (k) were determined. Line-shape simulation and k values of those of $\mathbf{1}_4$•**4a**, $\mathbf{2}_4$•**4a**, and $\mathbf{3a}_4$•**4a** are shown in Figure S25. Based on these data, the enthalpic ($\Delta H^{\ddagger}$) and entropic ($\Delta S^{\ddagger}$) contributions to the free energy of activation ($\Delta G^{\ddagger}$) and Arrhenius activation energies (E_a) for the rotational steric barriers of the four RhCl-tetraarylporphyrin subunits in (RhCl-tetraarylporphyrin)$_4$•**4a** were obtained by Eyring and Arrhenius plots, respectively (Figure S26). The results are summarized in Table 1. Comparison between the exchange rate constant for the rotation of RhCl-tetraarylporphyrin subunits on **4a** ($k > 10^4$

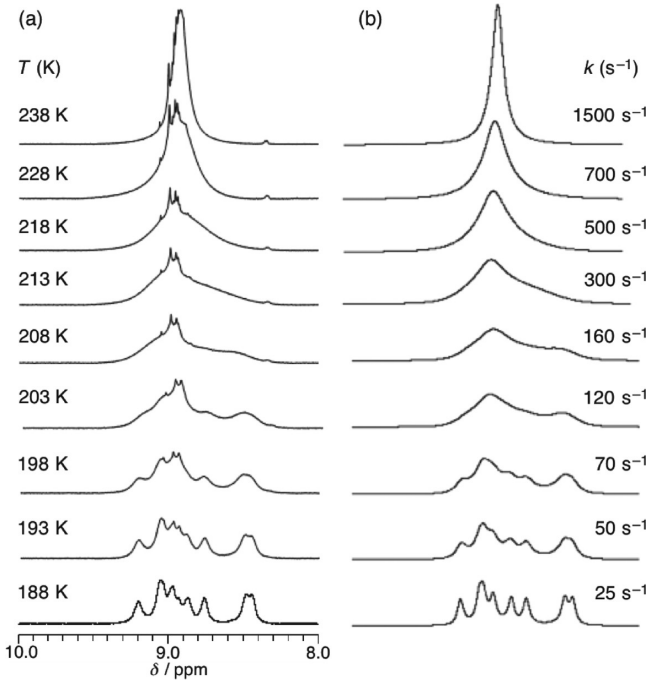

Figure 14. Temperature dependence of the ^{1}H NMR signal of the pyrrole-βH of $\mathbf{3b}_4$•**4a** (400 MHz, CD_2Cl_2): (a) observed spectra and (b) line-shape simulation. Values of temperature (T, K) and exchange rate constant (k, s^{-1}) are given for every trace.

s^{-1} at 298 K, derived from the Arrhenius equation and Figure S26) and that for the dissociation of RhCl-tetraarylporphyrin subunit from **4a** (k_{-1}) is important in supramolecular system because the rotation might proceed through a dissociation−association mechanism of the Rh−pyridyl axial coordination bond in (RhCl-tetraarylporphyrin)$_4$•**4a**. However, the k_{-1} value was too small and below the detection limits ($k_{-1} \ll 0.1$ s^{-1}) on

DOI: 10.1021/jacs.6b07284
J. Am. Chem. Soc. 2016, 138, 12564−12577

Table 1. Activation Parameters for the Rotation of Porphyrin Subunits in (RhCl-tetraarylporphyrin)$_4$•**4a** in CD_2Cl_2[a]

complex	E_a (kcal mol^{-1})	$\Delta H^{\ddagger}$ (kcal mol^{-1})	$\Delta S^{\ddagger}$ (cal K^{-1} mol^{-1})	$\Delta G^{\ddagger}$ at 188 K (kcal mol^{-1})	$\Delta G^{\ddagger}$ at 298 K (kcal mol^{-1})
1$_4$•**4a**	7.09	5.92	−17.25	9.16	11.06
2$_4$•**4a**	3.77	2.96	−28.87	8.38	11.56
3a$_4$•**4a**	6.49	5.38	−18.05	8.78	10.76
3b$_4$•**4a**	8.08	6.79	−15.05	9.62	11.28

[a]Values of E_a as well as those of $\Delta H^{\ddagger}$ and $\Delta S^{\ddagger}$ were obtained by Arrhenius and Eyring plots, respectively, based on the exchange rate constants derived from the line-shape analysis of the VT ^{1}H NMR spectra of the pyrrole-βH signals.

the NMR time scale even at 323 K, as mentioned above (Figure S12).[15] Thus, even if the dissociation of RhCl-tetraarylporphyrin subunit from **4a** occurs, the dissociation would be at least 5 orders of magnitude slower than the rotation of RhCl-tetraarylporphyrin subunits on **4a**. This result excludes a dissociation−association mechanism of the Rh−pyridyl coordination bond for the rotation of the four RhCl-tetraarylporphyrin subunits in (RhCl-tetraarylporphyrin)$_4$•**4a**.

In Table 1, the following features are noteworthy concerning the rotation of the four RhCl-tetraarylporphyrin subunits in (RhCl-tetraarylporphyrin)$_4$•**4a**.

Item 1. The $\Delta H^{\ddagger}$ and E_a decreased in the order **3b**$_4$•**4a** > **1**$_4$•**4a** > **3a**$_4$•**4a** > **2**$_4$•**4a**. In other words, from the viewpoint of the $\Delta H^{\ddagger}$ contribution, the four RhCl-tetraarylporphyrin subunits easily rotate in the order **3b**$_4$•**4a** < **1**$_4$•**4a** < **3a**$_4$•**4a** < **2**$_4$•**4a**.

Item 2. From the viewpoint of the $\Delta S^{\ddagger}$ contribution, the four RhCl-tetraarylporphyrin subunits easily rotate in the order **2**$_4$•**4a** < **3a**$_4$•**4a** < **1**$_4$•**4a** < **3b**$_4$•**4a**. The reverse of the order between $\Delta H^{\ddagger}$ and $\Delta S^{\ddagger}$ contributions to the free energy of the activation ($\Delta G^{\ddagger}$), namely, the rotational steric barriers of RhCl-tetraarylporphyrin subunits on **4a**, is considered as a result of enthalpy−entropy compensation.

Item 3. If the $\pi-\pi$ stacking and CH−π interactions between the cruciately interdigitating aryl groups (as shown by the X-ray structure in Figure 5) among adjacent RhCl-tetraarylporphyrin subunits are more effective in the ground state than in the activation state, then the $\Delta H^{\ddagger}$ value would become large. The negative $\Delta S^{\ddagger}$ values denote that the activation states are more ordered than the ground states, suggesting an existence of weak attractive interactions in the activation states between the adjacent RhCl-tetraarylporphyrin subunits. This may be related to the geared coupled rotation but not the slipping rotation. For **2**$_4$•**4a** as a tooth-expanded version, more disordered structures may be generated in the ground states by weakened $\pi-\pi$ stacking interactions, probably due to rotation of the *p*-methylphenyl moiety of the *p*-methylbiphenyl group (see signals E and F in Figures 7b and 8), leading to a smaller $\Delta H^{\ddagger}$ and a smaller (more negative) $\Delta S^{\ddagger}$. In contrast, for **3b**$_4$•**4a** as a sterically tooth-bulky version, the steric hindrance may be greater in the activation state than in the ground state since the bulky *n*-propoxy groups are substituted at the *meta*-positions of the aryl rings, leading to a relatively larger $\Delta H^{\ddagger}$ and a larger (less negative) $\Delta S^{\ddagger}$.

Item 4. The calculated free energy of activation ($\Delta G^{\ddagger} = \Delta H^{\ddagger} - T\Delta S^{\ddagger}$), namely, the rotational steric barriers of RhCl-tetraarylporphyrin subunits on **4a**, increased in the order **2**$_4$•**4a** < **3a**$_4$•**4a** < **1**$_4$•**4a** < **3b**$_4$•**4a** at 188 K. This tendency reflects splitting degrees of the ^{1}H NMR signals of the pyrrole-βHs of (RhCl-tetraarylporphyrin)$_4$•**4a** at 188 K, wherein no splitting for **2**$_4$•**4a** and **3a**$_4$•**4a**, some splitting for **1**$_4$•**4a**, and splitting in the seven signals for **3b**$_4$•**4a**, as mentioned above. On the other hand, $\Delta G^{\ddagger}$ increased in the order **3a**$_4$•**4a** < **1**$_4$•**4a** < **3b**$_4$•**4a** < **2**$_4$•**4a** at 298 K because of the contribution of the entropy term. This tendency somewhat reflects the sharpness of the ^{1}H NMR signal of the pyrrole-βH at 298 K, wherein the signal of **2**$_4$•**4a** was somewhat broadened, compared with those of **1**$_4$•**4a**, **3a**$_4$•**4a**, and **3b**$_4$•**4a**. This strongly implies that the activation characters obtained from the Eyring plots for the lower temperature region (118−230 K) are held even at the higher temperature region.

Item 5. The Arrhenius activation energies (E_a) for the rotational steric barriers of the four RhCl-tetraarylporphyrin subunits in (RhCl-tetraarylporphyrin)$_4$•**4a** were 3.8−8.1 kcal mol^{-1} and increased in the order **2**$_4$•**4a** < **3a**$_4$•**4a** < **1**$_4$•**4a** < **3b**$_4$•**4a**. For reference, these values are comparable to or lower than that of a RhCl-tetraarylporphyrin-based molecular gear[8a] and much lower than those of tripticene-based gear-slippage processes.[6a]

Item 6. The values of $\Delta G^{\ddagger}$ for the rotational steric barriers of the four RhCl-tetraarylporphyrin subunits in (RhCl-tetraarylporphyrin)$_4$•**4a** were 10.8−11.6 kcal mol^{-1} at 298 K. For reference, these values are lower than that of a RhCl-tetraarylporphyrin-based molecular gear[8a] and much lower than those of rotational barriers for the *p*-substituted-phenyl group rotations in metalated tetrakis(*p*-substituted-phenyl)-porphyrins bearing one or two axial ligands on the metal.[6b] Such substantially low activation barriers in the present systems would be explained by the above-mentioned attractive interactions in the activation states since this stabilization may contribute to the smaller $\Delta H^{\ddagger}$ together with the negative $\Delta S^{\ddagger}$.

Item 7. In general, it is known that $\Delta G^{\ddagger}(E_a)$ of slipping rotation is much greater than that of geared rotation.[6a] Despite large differences of aryl groups as teeth of gear wheels among **1**$_4$•**4a**, **2**$_4$•**4a**, **3a**$_4$•**4a**, and **3b**$_4$•**4a**, the differences of $\Delta G^{\ddagger}$ values among them were very small within the range of only 0.80 kcal mol^{-1} at 298 K (11.06 kcal mol^{-1} for **1**$_4$•**4a** vs maximum = 11.56 kcal mol^{-1} for **2**$_4$•**4a** and minimum = 10.76 kcal mol^{-1} for **3a**$_4$•**4a**) and within the range of only 1.24 kcal mol^{-1} at 188 K (9.16 kcal mol^{-1} for **1**$_4$•**4a** vs maximum = 9.62 kcal mol^{-1} for **3b**$_4$•**4a** and minimum = 8.38 kcal mol^{-1} for **2**$_4$•**4a**). If **2**$_4$•**4a** as a tooth-expanded version of **1**$_4$•**4a** and **3b**$_4$•**4a** as a sterically tooth-bulky version of **1**$_4$•**4a** obey a slipping rotation mechanism, then $\Delta G^{\ddagger}$ values of **2**$_4$•**4a** and **3b**$_4$•**4a** should be much greater than that of **1**$_4$•**4a**. However, the differences of $\Delta G^{\ddagger}$ values among them were very small in practice. The $\Delta G^{\ddagger}$ value of **1**$_4$•**4a** was in between those of **2**$_4$•**4a** and **3b**$_4$•**4a** at 188 K and was only slightly lower than those of **3b**$_4$•**4a** ($\Delta\Delta G^{\ddagger}$ = 0.22 kcal mol^{-1}) and **2**$_4$•**4a** ($\Delta\Delta G^{\ddagger}$ = 0.50 kcal mol^{-1}) at 298 K.

Thus, these results clearly exclude a slipping rotation mechanism. Judging from these results in a comprehensive manner, we conclude that **1**$_4$•**4a**, **2**$_4$•**4a**, **3a**$_4$•**4a**, and **3b**$_4$•**4a** in solution obey a geared coupled rotation mechanism and behave as quadruple interlocking gears, wherein one subunit-**1** (**2**, **3a**,

DOI: 10.1021/jacs.6b07284
J. Am. Chem. Soc. 2016, 138, 12564−12577

and **3b**) and two adjacent subunits-**1** (**2**, **3a**, and **3b**) have to interlock with cooperative, mutually inverse rotation (Figure 5d).

CONCLUSIONS

We have demonstrated that four molecules of Rh(III)Cl *meso*-tetraarylporphyrins and one molecule of bowl-shaped tetra(*p*-pyridyl)cavitand derivatives self-assemble into 4:1 complexes in $CDCl_3$ via Rh−pyridyl axial coordination bonds. This is a new molecular gear system coupled with four gear wheels. Complexes of $\mathbf{1}_4$•**4a**, $\mathbf{2}_4$•**4a**, $\mathbf{3a}_4$•**4a**, and $\mathbf{3b}_4$•**4a** derived from Rh(III)Cl *meso*-tetrakis(4-methylphenyl)porphyrin **1**, Rh(III)Cl *meso*-tetrakis[4-(4-methylphenyl)phenyl]porphyrin **2**, Rh(III)Cl *meso*-tetrakis(3,5-dimethoxyphenyl)porphyrin **3a**, or Rh(III)Cl *meso*-tetrakis(3,5-di-*n*-propoxyphenyl)porphyrin **3b** and tetra(4-pyridyl)cavitand **4a** (R = $(CH_2)_6CH_3$) behaved as a quadruple interlocking gear with an inner space, wherein four subunits-**1**, -**2**, and -**3** are gear wheels, their four aryl groups at the *meso*-positions are the teeth moieties of the gear wheels, and four *p*-pyridyl groups in the subunit-**4a** are axes of gear wheels. The extremely strong porphyrin-Rh−pyridyl axial coordination bond, the rigidity of the methylene-bridge cavitand as a scaffold of the pyridyl axes, and the cruciform arrangement of four sets of the interdigitating aryl groups as the teeth moieties of the gear wheels in the assembling (RhCl-tetraarylporphyrin)$_4$-unit made $\mathbf{1}_4$•**4a**, $\mathbf{2}_4$•**4a**, $\mathbf{3a}_4$•**4a**, and $\mathbf{3b}_4$•**4a** function as a quadruple interlocking gear in solution, namely, having no slipping rotation mechanism. The results of activation parameters ($\Delta H^{\ddagger}$, $\Delta S^{\ddagger}$, and $\Delta G^{\ddagger}$) obtained from Eyring plots based on line-shape analysis of the VT ^{1}H NMR spectra of $\mathbf{1}_4$•**4a**, $\mathbf{2}_4$•**4a**, $\mathbf{3a}_4$•**4a**, and $\mathbf{3b}_4$•**4a** supported the interlocking rotation (geared coupled rotation) mechanism. Despite large differences of aryl groups as teeth of gear wheels among $\mathbf{1}_4$•**4a**, $\mathbf{2}_4$•**4a** (a tooth-expanded version of $\mathbf{1}_4$•**4a**), $\mathbf{3a}_4$•**4a**, and $\mathbf{3b}_4$•**4a** (a sterically tooth-bulky version of $\mathbf{1}_4$•**4a**), the differences of $\Delta G^{\ddagger}$ values among them were very small, within the range of only 0.80 kcal mol^{-1} at 298 K and within the range of only 1.24 kcal mol^{-1} at 188 K.

The single-crystal X-ray diffraction analysis of $\mathbf{1}_4$•**4b** (R = $CH_2CH(CH_3)_2$) indicated chiral space group *I*4, wherein (i) the regular interdigitation of inwardly oriented *p*-tolyl groups of the four achiral subunits-**1** made the arrangement of the assembling $\mathbf{1}_4$-unit chiral, (ii) all $\mathbf{1}_4$•**4b** were unidirectionally aligned along the *c*-axis, and (iii) $\mathbf{1}_4$•**4b** encapsulated at least three molecules of EtOH upon recrystallization.

Thus, we can put four gear wheels **1**−**3** simultaneously on a platform **4** in a proximate fashion to construct quadruple interlocking gears. Studies on (i) searching for a guest molecule that can be encapsulated in $\mathbf{1}_4$•**4a**, $\mathbf{2}_4$•**4a**, and $\mathbf{3}_4$•**4a** and (ii) control of the gear-rotation behavior of them by an external stimulus such as a guest addition[9,11] are currently under way in our laboratory.

ASSOCIATED CONTENT

Supporting Information

The Supporting Information is available free of charge on the ACS Publications website at DOI: 10.1021/jacs.6b07284.

Experimental details and additional data (PDF)

Crystallographic information file for $\mathbf{1}_4$•**4b** (CIF)

AUTHOR INFORMATION

Corresponding Authors

*kobayashi.kenji.a@shizuoka.ac.jp

*ykobori@kitty.kobe-u.ac.jp

Notes

The authors declare no competing financial interest.

ACKNOWLEDGMENTS

This work was supported in part by Grant-in-Aid from JSPS (no. 25288034 to K. Kobayashi).

REFERENCES

(1) (a) Satake, A.; Kobuke, Y. *Tetrahedron* **2005**, *61*, 13−41. (b) Drain, C. M.; Varotto, A.; Radivojevic, I. *Chem. Rev.* **2009**, *109*, 1630−1658. (c) Beletskaya, I.; Tyurin, V. S.; Tsivadze, A. Y.; Guilard, R.; Stern, C. *Chem. Rev.* **2009**, *109*, 1659−1713. (d) Aratani, N.; Kim, D.; Osuka, A. *Acc. Chem. Res.* **2009**, *42*, 1922−1934. (e) Durot, S.; Taesch, J.; Heitz, V. *Chem. Rev.* **2014**, *114*, 8542−8578.

(2) (a) Anderson, S.; Anderson, H. L.; Sanders, J. K. M. *Acc. Chem. Res.* **1993**, *26*, 469−475. (b) Anderson, S.; Anderson, H. L.; Bashall, A.; McPartlin, M.; Sanders, J. K. M. *Angew. Chem., Int. Ed. Engl.* **1995**, *34*, 1096−1099. (c) Yong, C.-K.; Parkinson, P.; Kondratuk, D. V.; Chen, W.-H.; Stannard, A.; Summerfield, A.; Sprafke, J. K.; O'Sullivan, M. C.; Beton, P. H.; Anderson, H. L.; Herz, L. M. *Chem. Sci.* **2015**, *6*, 181−189. (d) Liu, S.; Kondratuk, D. V.; Rousseaux, S. A. L.; Gil-Ramírez, G.; O'Sullivan, M. C.; Cremers, J.; Claridge, T. D. W.; Anderson, H. L. *Angew. Chem., Int. Ed.* **2015**, *54*, 5355−5359.

(3) (a) Felluga, F.; Tecilla, P.; Hillier, L.; Hunter, C. A.; Licini, G.; Scrimin, P. *Chem. Commun.* **2000**, 1087−1088. (b) Ikeda, A.; Sonoda, K.; Shinkai, S. *Chem. Lett.* **2000**, *29*, 1220−1221. (c) Kaur, T.; Rajeswararao, M.; Ravikanth, M. *Inorg. Chem.* **2014**, *53*, 11051−11059.

(4) (a) Kim, H.-J.; Redman, J. E.; Nakash, M.; Feeder, N.; Teat, S. J.; Sanders, J. K. M. *Inorg. Chem.* **1999**, *38*, 5178−5183. (b) Kim, H.-J.; Bampos, N.; Sanders, J. K. M. *J. Am. Chem. Soc.* **1999**, *121*, 8120−8121. (c) Redman, J. E.; Feeder, N.; Teat, S. J.; Sanders, J. K. M. *Inorg. Chem.* **2001**, *40*, 2486−2499.

(5) (a) Alessio, E.; Macchi, M.; Heath, S.; Marzilli, L. G. *Chem. Commun.* **1996**, 1411−1412. (b) Kariya, N.; Imamura, T.; Sasaki, Y. *Inorg. Chem.* **1997**, *36*, 833−839. (c) Alessio, E.; Geremia, S.; Mestroni, S.; Srnova, I.; Slouf, M.; Gianferrara, T.; Prodi, A. *Inorg. Chem.* **1999**, *38*, 2527−2529. (d) Prodi, A.; Indelli, M. T.; Kleverlaan, C. J.; Scandola, F.; Alessio, E.; Gianferrara, T.; Marzilli, L. G. *Chem. - Eur. J.* **1999**, *5*, 2668−2679. (e) Iengo, E.; Zangrando, E.; Alessio, E. *Acc. Chem. Res.* **2006**, *39*, 841−851. (f) Indelli, M. T.; Chiorboli, C.; Ghirotti, M.; Orlandi, M.; Scandola, F.; Kim, H. J.; Kim, H.-J. *J. Phys. Chem. B* **2010**, *114*, 14273−14282.

(6) For reviews of molecular machines, see (a) Iwamura, H.; Mislow, K. *Acc. Chem. Res.* **1988**, *21*, 175−182. (b) Kottas, G. S.; Clarke, L. I.; Horinek, D.; Michl, J. *Chem. Rev.* **2005**, *105*, 1281−1376. (c) Kinbara, K.; Aida, T. *Chem. Rev.* **2005**, *105*, 1377−1400. (d) Khuong, T.-A. V.; Nunez, J. E.; Godinez, C. E.; Garcia-Garibay, M. A. *Acc. Chem. Res.* **2006**, *39*, 413−422. (e) Saha, S.; Stoddart, J. F. *Chem. Soc. Rev.* **2007**, *36*, 77−92. (f) Champin, B.; Mobian, P.; Sauvage, J.-P. *Chem. Soc. Rev.* **2007**, *36*, 358−366. (g) Kay, E. R.; Leigh, D. A.; Zerbetto, F. *Angew. Chem., Int. Ed.* **2007**, *46*, 72−191. (h) Feringa, B. L. *J. Org. Chem.* **2007**, *72*, 6635−6652. (i) Vives, G.; de Rouville, H.-P. J.; Carella, A.; Launay, J.-P.; Rapenne, G. *Chem. Soc. Rev.* **2009**, *38*, 1551−1561. (j) Thanasekaran, P.; Huang, C.-Y.; Lu, K.-L. *Chem. Lett.* **2013**, *42*, 776−784. (k) Niess, F.; Duplan, V.; Sauvage, J.-P. *Chem. Lett.* **2014**, *43*, 964−974. (l) Erbas-Cakmak, S.; Leigh, D. A.; McTernan, C. T.; Nussbaumer, A. L. *Chem. Rev.* **2015**, *115*, 10081−10206.

(7) For Rh(III)Cl tetraarylporphyrin-based rotaxane, see Asakawa, M.; Ikeda, T.; Yui, N.; Shimizu, T. *Chem. Lett.* **2002**, *31*, 174−175.

(8) For Rh(III)Cl tetraarylporphyrin-based molecular gears, see (a) Ogi, S.; Ikeda, T.; Wakabayashi, R.; Shinkai, S.; Takeuchi, M. *Chem. - Eur. J.* **2010**, *16*, 8285−8290. (b) Ogi, S.; Ikeda, T.;

DOI: 10.1021/jacs.6b07284
J. Am. Chem. Soc. 2016, 138, 12564−12577

Wakabayashi, R.; Shinkai, S.; Takeuchi, M. *Eur. J. Org. Chem.* **2011**, *2011*, 1831−1836.
(9) For tetraarylprophyrin-based multicomponent supramolecular rotors, see (a) Samanta, S. K.; Schmittel, M. *J. Am. Chem. Soc.* **2013**, *135*, 18794−18797. (b) Samanta, S. K.; Rana, A.; Schmittel, M. *Angew. Chem., Int. Ed.* **2016**, *55*, 2267−2272.
(10) (a) Hiraoka, S.; Okuno, E.; Tanaka, T.; Shiro, M.; Shionoya, M. *J. Am. Chem. Soc.* **2008**, *130*, 9089−9098. (b) Hiraoka, S.; Hisanaga, Y.; Shiro, M.; Shionoya, M. *Angew. Chem., Int. Ed.* **2010**, *49*, 1669−1673.
(11) Sanada, K.; Ube, H.; Shionoya, M. *J. Am. Chem. Soc.* **2016**, *138*, 2945−2948.
(12) (a) Kobayashi, K.; Yamada, Y.; Yamanaka, M.; Sei, Y.; Yamaguchi, K. *J. Am. Chem. Soc.* **2004**, *126*, 13896−13897. (b) Kitagawa, H.; Kobori, Y.; Yamanaka, M.; Yoza, K.; Kobayashi, K. *Proc. Natl. Acad. Sci. U. S. A.* **2009**, *106*, 10444−10448. (c) Kobayashi, K.; Yamanaka, M. *Chem. Soc. Rev.* **2015**, *44*, 449−466 and references cited therein.
(13) Chan, K. S.; Lau, C. M. *Organometallics* **2006**, *25*, 260−265.
(14) The chemical shift of the Pyα-proton of the subunit-**4a** in **1**$_4$•**4a** was somewhat shifted downfield ($\Delta\delta$ = ca. 0.1 ppm) with increasing the solution temperature, probably because of the effect of rapid rotation about the C−C bond between the porphyrin ring and the *p*-tolyl group on the NMR time scale at higher temperature.
(15) Gunter, M. J.; Bampos, N.; Johnstone, K. D.; Sanders, J. K. M. *New J. Chem.* **2001**, *25*, 166−173. (In this work, association constants (K_a) and off-rate constants (k_{-1}) of metallo-tetraarylporphyrins and pyridine in $CDCl_3$ at room temperature are shown: Zn-porphyrin: K_a = 10^3−10^4 M^{-1} and k_{-1} = ca. 10^5 s^{-1}; Ru(CO)-porphyrin: K_a = 10^7−10^8 M^{-1} and k_{-1} = ca. 0.1 s^{-1}; RhI-porphyrin: K_a > 10^9 M^{-1} (probably, k_{-1} < 0.1 s^{-1}).)
(16) In marked contrast to the very stable Rh−pyridyl axial coordination bond in **1**$_4$•**4a**, the Zn−pyridyl axial coordination bond in **1**-Zn$_4$•**4a** was not so stable,[15] wherein the $\Delta\delta$ values of the ^{1}H NMR signals of the Pyα-proton (a) and Pyβ-proton (b) of subunit-**4a** were −4.06 and −1.46 ppm, respectively, under the conditions [**1**-Zn] = 8 mM and [**4a**] = 2 mM in $CDCl_3$ at 298 K (Figure S11).
(17) (a) Feringa, B. L.; van Delden, R. A. *Angew. Chem., Int. Ed.* **1999**, *38*, 3418−3438. (b) Matsuura, T.; Koshima, H. *J. Photochem. Photobiol., C* **2005**, *6*, 7−24. (c) Sögütoglu, L.-C.; Steendam, R. R. E.; Meekes, H.; Vlieg, E.; Rutjes, F. P. J. T. *Chem. Soc. Rev.* **2015**, *44*, 6723−6732.
(18) (a) Azumaya, I.; Yamaguchi, K.; Okamoto, I.; Kagechika, H.; Shudo, K. *J. Am. Chem. Soc.* **1995**, *117*, 9083−9084. (b) Ezuhara, T.; Endo, K.; Aoyama, Y. *J. Am. Chem. Soc.* **1999**, *121*, 3279−3283.
(19) Seibel, J.; Parschau, M.; Ernst, K.-H. *J. Am. Chem. Soc.* **2015**, *137*, 7970−7973.
(20) The ^{1}H NMR signal of the Pyα-proton (a) of **2**$_4$•**4a** was overlapped with those of the alkyl side chain (i−k) and was assigned by the ^{1}H−^{1}H COSY spectrum (Figure S15).
(21) The ^{1}H NMR signal of the Pyα-proton (a) of **3b**$_4$•**4a** was partially overlapped with that of the terminal methyl group (m) of the alkyl side chain and was assigned by the ^{1}H−^{1}H COSY spectrum (Figure S19).

DOI: 10.1021/jacs.6b07284
J. Am. Chem. Soc. 2016, 138, 12564−12577